

Discovery of period doubling in BL Herculis stars of the OGLE survey. Observations and theoretical models.

R. Smolec^{1*}, I. Soszyński², P. Moskalik³, A. Udalski², M. K. Szymański²,
M. Kubiak², G. Pietrzyński^{2,4}, Ł. Wyrzykowski^{2,5}, K. Ulaczyk², R. Poleski²,
S. Kozłowski² and P. Pietrukowicz²

¹*Institute for Astronomy (IfA), University of Vienna, Türkenschanzstrasse 17, A-1180 Wien, Austria*

²*Warsaw University Observatory, Al. Ujazdowskie 4, 00-478 Warszawa, Poland*

³*Copernicus Astronomical Centre, Bartycka 18, 00-716 Warszawa, Poland*

⁴*Universidad de Concepción, Departamento de Astronomía, Casilla 160??C, Concepción, Chile*

⁵*Institute of Astronomy, University of Cambridge, Madingley Road, Cambridge CB3 0HA, UK*

Accepted . Received ; in original form

ABSTRACT

We report the discovery of a period doubling behaviour in a 2.4 d BL Herculis-type variable of the Galactic bulge. Another bulge BL Her-type star ($P = 2.25$ d) is a strong period doubling candidate. Both objects have been identified with the OGLE-III photometry. Possibility of period doubling in this type of pulsators has been predicted almost twenty years ago by Buchler & Moskalik (1992). Our finding is the first observational confirmation of their theoretical results.

Discovery of the first BL Herculis star showing the period doubling effect motivates a new theoretical investigation with the state-of-the-art convective pulsation codes. We present the results of initial model survey, specifically aimed at studying the observed period-doubled BL Her variable. All of our non-linear models have $P = 2.4$ d. The computations confirm that the period doubling effect is caused by the 3:2 resonance between the fundamental mode and the first overtone, as indicated by earlier radiative models of Buchler & Moskalik. Comparison of the computed and the observed light curves allows to constrain the parameters of the star, in particular its metallicity, which appears to be high, $Z \approx 0.01$. The recent evolutionary tracks put also constraint on the mass of the star, which is close to $M = 0.50 M_{\odot}$.

Key words: stars: variables: Cepheids – stars: Population II – stars: oscillations – hydrodynamics – stars: individual: BLG184.7133264 – stars: individual: BLG189.6137529

1 INTRODUCTION

BL Herculis-type variables are short-period (1 – 4 d) subgroup of the Type II (or Population II) Cepheids. They are predominantly found in the old stellar populations, in the globular clusters and in the Galactic halo. They are believed to be low-mass stars evolving away from the Zero-Age Horizontal Branch (ZAHB) towards the Asymptotic Giant Branch (AGB), crossing the instability strip (IS) at luminosities larger than RR Lyrae stars (Strom et al. 1970; Gingold 1985, see also Section 4). All Type II Cepheids, including BL Her variables, obey a well defined period-luminosity relation and can be used as distance indicators

(e.g. Majaess et al. 2009a,b, and references therein). They are also key objects for studying the stellar and galactic evolution (see e.g., Wallerstein 2002).

Characteristic feature of the BL Her light curves is a secondary bump observed in some of the variables. The phenomenon is similar to the Hertzsprung bump progression observed in the classical, Population I Cepheids and is also interpreted as caused by the resonant interaction between the fundamental mode and the second overtone (Hodson, Cox & King 1982). Some early hydrodynamic models of BL Her variables were computed by e.g. Hodson, Cox & King (1982) and Carson & Stothers (1982). Fadeyev & Fokin (1985) computed several Type II Cepheid models, including BL Her models. One of their models revealed oscillations with alternating amplitude and period.

* E-mail: radek.smolec@univie.ac.at

A large and systematic survey of the radiative BL Her models was conducted by Buchler & Moskalik (1992) and Moskalik & Buchler (1993a). In most of their model sequences Buchler & Moskalik (1992) found narrow windows of parameters for which the light and radial velocity curves exhibited a periodic alternations of deep and shallow minima – the period doubling effect. The origin of the period doubling in hydrodynamic models was traced by Moskalik & Buchler (1990) to the destabilising role of the half-integer resonances, $(2n + 1)\omega_0 = 2\omega_k$, between the fundamental mode and the higher order overtones. Close to the resonance centre period-doubling bifurcation can occur: the fundamental mode limit cycle becomes unstable, and period-two solution, with alternating shape of the light and radial velocity curves can emerge. Buchler & Moskalik (1992) (see also Moskalik & Buchler 1993b) showed that their BL Her models undergo a period-doubling bifurcation caused by the 3:2 resonance between the fundamental mode and the first overtone. Buchler & Moskalik (1992) concluded that period doubling effect, not observed in any BL Her star at that time, should be eventually found. More recently, Marconi & Di Criscienzo (2007) conducted a large survey of BL Her-type convective models, however none of their models exhibited period doubling.

Alternating deep and shallow minima are characteristic feature of RV Tau-type variables, which, together with W Vir-type stars, form another subgroup of the Type II Cepheids (for recent review see e.g., Wallerstein 2002; Szabados 2010). These longer period variables (periods of $\sim 4 - 20$ d for W Vir stars and above ~ 20 d for RV Tau stars) are more evolutionary advanced than the BL Her variables. The W Vir stars loop into the instability strip during the helium-shell flashes, while climbing up along the AGB, whereas the RV Tau stars enter the instability strip evolving away from the AGB toward a white dwarf domain. Period doubling behaviour appears first at $P \simeq 19 - 20$ d; this is a borderline between the W Vir and RV Tau classes. However, the two classes overlap in period and the distinction between them is not clear-cut (e.g., Szabados 2010; Wils & Otero 2008). The RV Tau behaviour was reproduced in the radiative hydrodynamic models of Buchler & Kovács (1987) and Kovács & Buchler (1988). As analysed later by Moskalik & Buchler (1990), the period doubling in these models is caused by the 5:2 resonance between the fundamental mode and the second overtone.

Period doubling was also discovered in the *Kepler* observations of RR Lyrae stars exhibiting the Blazhko phenomenon (Kolenberg et al. 2010; Szabó et al. 2010). However, to the present day period doubling was not detected in any BL Her-type star, despite theoretical predictions.

In this paper we report the discovery of the first BL Her variable clearly showing the period doubling phenomenon as predicted by the theoretical models. The star was found during the preparation of the subsequent part of the OGLE-III Catalogue of Variable Stars (OIII-CVS), devoted to the Type II Cepheids in the Galactic bulge (Soszyński et al. 2011, in prep.). In Section 2 we present and analyse the light curve of the star and prove that it is indeed a BL Her-type pulsator. We also discuss another candidate in which period doubling is strongly suspected, for which however, definite claims require more precise photometric observations.

In Section 3 we present a new set of non-linear hydro-

dynamic models. As compared to the Moskalik & Buchler (1993a) models, these models are convective and include up to date physics. Our efforts focus on modelling the single BL Her star with unambiguously detected period doubling. In majority of our model sequences we find the period doubling domains and show that they originate from the resonant interaction of the fundamental mode with the first overtone, corroborating the earlier result of Buchler & Moskalik (1992). Comparison of the model and observed light curves allows to constrain the parameters of the star (mass, luminosity and metallicity). In Section 4 we confront these parameters with the predictions of the stellar evolution theory. We discuss our results and summarise the conclusions in Section 5.

2 OBSERVATIONS AND DATA ANALYSIS

In this study we used Cousins *I*-band photometry of the Galactic bulge, obtained during the third phase of the Optical Gravitational Lensing Experiment (OGLE-III). The observations were collected between 2001 and 2009, with the 1.3 m Warsaw telescope located at Las Campanas Observatory, Chile. A limited number of measurements in Johnson’s *V*-band was also obtained to determine (*V* – *I*) colour of the stars. The photometry was reduced with the Difference Image Analysis method (DIA, Alard & Lupton 1998; Woźniak 2000). Detailed description of the OGLE-III instrumental setup and data reduction procedures can be found in Udalski (2003) and Udalski et al. (2008).

During the preparation of the catalogue of Type II Cepheids in the Galactic bulge (Soszyński et al. 2011, in prep.), two BL Her stars with unusual properties were identified. Both objects display excessive scatter around the light curve maxima and minima. This attracted our attention, and prompted thorough investigation of these two variables.

2.1 BLG184.7 133264 : first BL Herculis-type star with period doubling

The OGLE-III *I*-band photometry of BLG184.7 133264 (18:02:56.60, –30:42:34.4) consists of 768 measurements, spanning 2830 d. We analysed these data using a standard consecutive pre-whitening technique. The star displays a very pronounced variability with the period of $P_0 = 2.399267$ d ($f_0 = 0.4167939$ d^{–1}). We fitted this variability with the Fourier series of the form:

$$I(t) = I_0 + \sum_k A_k \cos(2\pi k f_0 t + \phi_k), \quad (1)$$

where the frequency f_0 was also optimised. In the next step, we subtracted the fitted function from the light curve (“pre-whitening”), and then searched the residuals for additional periodicities. This was done with the standard Fourier power spectrum. In Fig. 1 we present the results of this procedure. The power spectrum of the pre-whitened data (second panel of the figure) is dominated by a peak at $f_x = 0.20841$ d^{–1}. Within accuracy of the data, this frequency is identical to $1/2 f_0$. In other words, f_x is a *subharmonic* of the primary pulsation frequency f_0 . Subsequent step by step pre-whitening revealed additional subharmonics, up to $9/2 f_0$

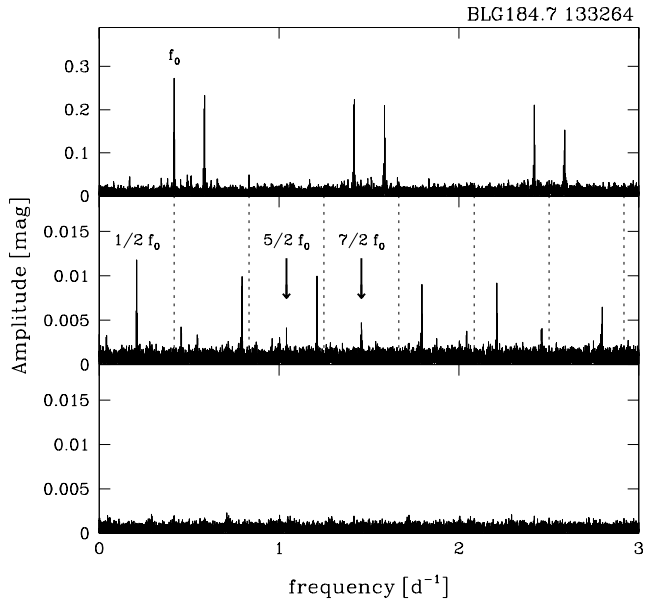


Figure 1. Pre-whitening sequence for BLG184.7 133264. Upper panel: power spectrum of original data. The spectrum is dominated by pulsation frequency f_0 and its daily aliases. Middle panel: power spectrum after removing f_0 and its harmonics. Dashed lines indicate locations of the pre-whitened frequencies. The highest peak corresponds to a subharmonic frequency, $1/2 f_0$, its daily aliases are very prominent, too. Two other subharmonic frequencies ($5/2 f_0$ and $7/2 f_0$) are also visible. Lower panel: power spectrum after removing f_0 , its harmonics and its subharmonics.

($5/2 f_0$ and $7/2 f_0$ are noticeable already in Fig. 1). No other secondary periodicities were found.

The presence of subharmonic frequencies in the power spectrum, i.e. frequencies of the form $(n+1/2)f_0$, is a characteristic signature of a period doubling. In the time domain it means that the light curve of the star is still *strictly periodic*, but it repeats itself not after one, but after *two* pulsation periods. In other words, the light curve displays regular alternations of higher and lower maxima (and minima). This is clearly visible in Fig. 2, where we plot the light curve of BLG184.7 133264 folded with twice the pulsation period ($2P_0$). The difference between the two consecutive maxima is small (0.020 mag), nevertheless well visible. Such alternating light curves are well known in longer period W Vir and RV Tau variables ($P_0 > 19 - 20$ d, see Wils & Otero 2008), but they were never before observed in the BL Her stars. BLG184.7 133264 is the first BL Her-type variable, in which period doubling is unambiguously detected.

To fully characterise the light curve of BLG184.7 133264, we fitted the data with the final Fourier series, which included all the detected subharmonics:

$$I(t) = I_0 + \sum_k A_k \cos(2\pi k f_0 t + \phi_k) + \sum_n B_{n+1/2} \cos[2\pi(n+1/2)f_0 t + \psi_{n+1/2}]. \quad (2)$$

This function is plotted in Fig. 2, together with the folded photometric data. The amplitude of the main pulsation component is $A_1 = 0.2742 \pm 0.0005$ mag. The highest subhar-

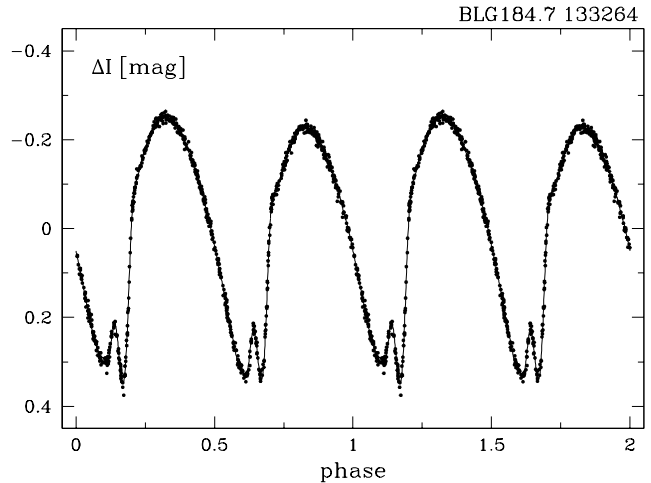


Figure 2. Light curve of BLG184.7 133264 folded with twice the pulsation period, $2P_0$.

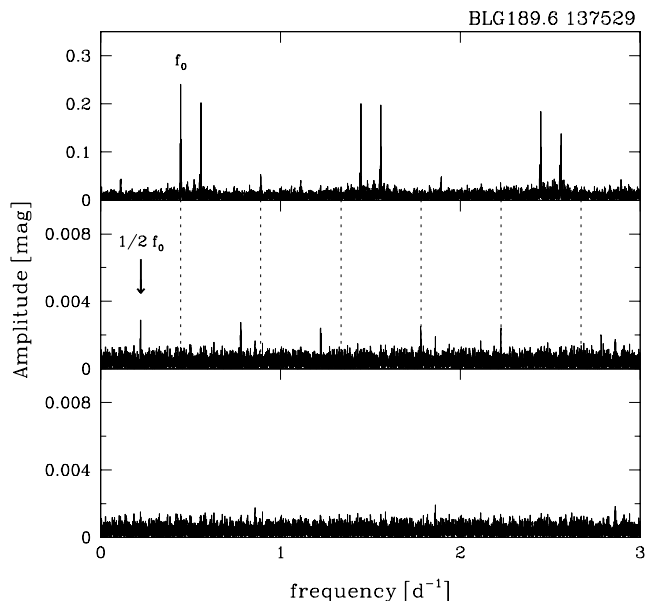


Figure 3. Pre-whitening sequence for BLG189.6 137529. Upper panel: power spectrum of original data. The spectrum is dominated by pulsation frequency f_0 and its daily aliases. Middle panel: power spectrum after removing f_0 and its harmonics. Dashed lines indicate locations of the pre-whitened frequencies. The highest peak corresponds to a subharmonic frequency, $1/2 f_0$, its daily aliases are also visible. Lower panel: power spectrum after removing f_0 , its harmonics and its subharmonics.

monic is over twenty times smaller and has an amplitude of $B_{1/2} = 0.0127 \pm 0.0005$ mag. The power spectrum of residuals of the fit is displayed in the lower panel of Fig. 1. The dispersion of the residuals is $\sigma = 0.0086$ mag.

2.2 BLG189.6 137529 : period doubling candidate

BLG189.6 137529 (18:00:48.31, $-29:58:54.4$) is another BL Her variable in the Galactic bulge, pulsating with the period of $P_0 = 2.245688$ d ($f_0 = 0.4452978$ d $^{-1}$). During almost 8 years of OGLE-III observations the pulsation period

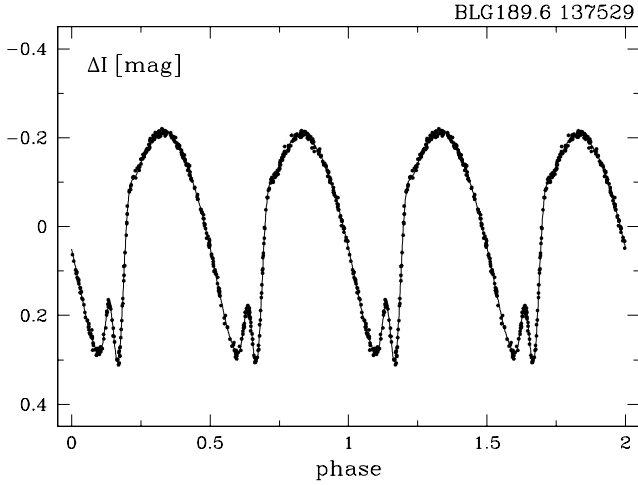


Figure 4. Light curve of BLG189.6 137529 folded with twice the pulsation period, $2P_0$.

of the star was slowly changing. Therefore, we decided to use in the analysis only a subset of data spanning 1540 d, from HJD = 2453416 to 2454956 (543 measurements in total). The data was analysed in the same way as in the previous case.

The pre-whitening sequence of BLG189.6 137529 is displayed in Fig. 3. Only one secondary peak was detected in this star. Its frequency, $f_x = 0.22257 \text{ d}^{-1}$, corresponds $1/2 f_0$. Thus, BLG189.6 137529 shows a signature of a period doubling. This time however, the detected subharmonic is extremely weak, with the amplitude of only $B_{1/2} = 0.0029 \pm 0.0004 \text{ mag}$. The light curve of BLG189.6 137529, folded with twice the pulsation period is displayed in Fig. 4. As we might have expected, the alternations of maxima and of minima are barely visible.

To make them visible better, we display the same data again in Fig. 5, but this time we do it differently. We plot the folded data twice, with different colours. The two curves are shifted by one pulsation period (i.e. by P_0). In this way, even and odd pulsation cycles are plotted on top of each other. The inset provides a closer look at the maxima of the folded curves. The red points are systematically higher than the black ones, but the difference is very small. The maxima of the fit lines differ by only 0.0058 mag, which is less than the scatter of the data around the fit (0.0064 mag).

Both Fig. 3 and Fig. 5 show that the period doubling in BLG189.6 137529, is present, but is much less significant than in the first star. We consider this BL Her variable to be a strong period doubling candidate, which however needs further confirmation with additional data. Such data are currently being collected (for both stars of this paper) within the fourth phase of the OGLE project.

2.3 Are BLG184.7 133264 and BLG189.6 137529 genuine BL Her-type variables ?

In Fig. 6 we put BLG184.7 133264 and BLG189.6 137529 on the colour-magnitude diagram, together with almost 17000 RR Lyr variables observed toward the Galactic bulge (Soszyński et al. 2011). The bulge RR Lyr stars are spread over a wide range of $(V - I)$ colours. This is caused by

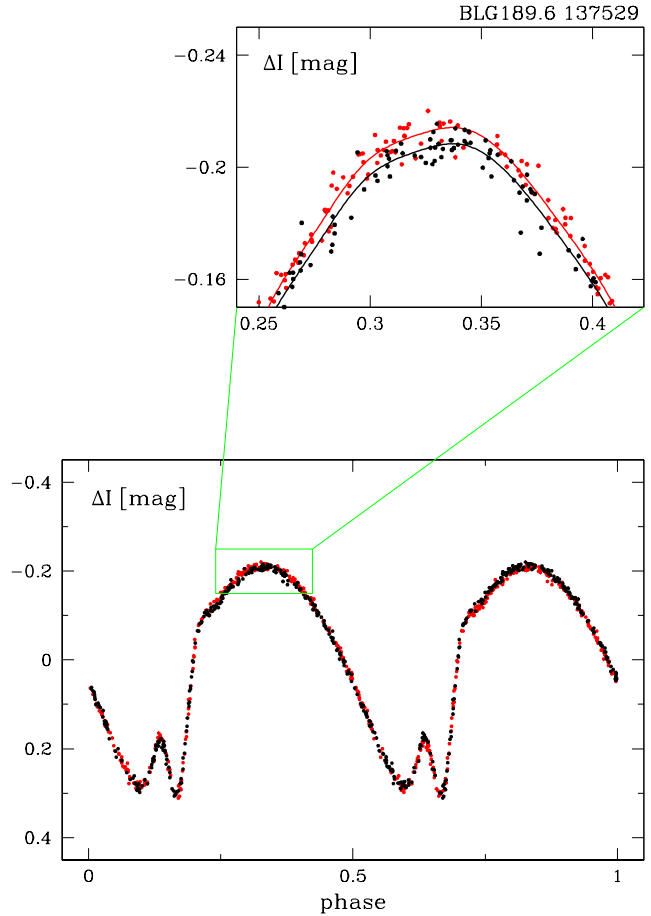


Figure 5. Light curve of BLG189.6 137529 folded with $2P_0$, plotted twice with different colours. The red and black curves are shifted by P_0 . The inset shows the difference between even and odd pulsation cycles.

Table 1. Light curves of BLG184.7 133264 and BLG189.6 137529.

	BLG184.7 133264	BLG189.6 137529
P_0 [d]	2.399267	2.245688
A_1 [mag]	0.2742	0.2438
$B_{1/2}$ [mag]	0.0127	0.0029
σ [mag]	0.0086	0.0064
R_{21}	0.216	0.190
R_{31}	0.076	0.071
ϕ_{21}	5.461	5.590
ϕ_{31}	3.994	3.908

large field-to-field variations of interstellar reddening. We plot with the filled circles the RRab stars located in the same fields as BLG184.7 133264 and BLG189.6 137529. Both period-doubled variables discussed in the current paper have the same colours as the RRab stars in their respective fields (i.e. RRab stars with the same reddening). This implies that BLG184.7 133264 and BLG189.6 137529 are located inside the instability strip. Their luminosities, which are $1.65 \pm 0.55 \text{ mag}$ brighter than the Horizontal Branch, place them in the domain of the BL Her-type pulsators.

The light curves of both stars are also quite typical

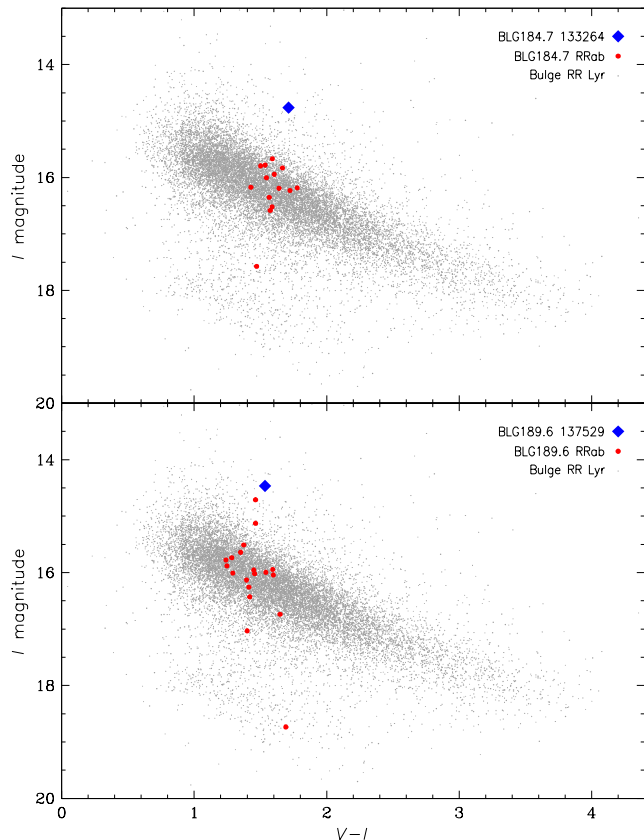


Figure 6. Colour-magnitude diagram for BLG184.7 133264 and BLG189.6 137529 (plotted with diamonds). Background grey dots represent RR Lyr stars observed toward the Galactic bulge. Filled circles mark RRab stars observed in the same fields as BLG184.7 133264 and BLG189.6 137529.

for the BL Her variables. In Fig. 7 we display a selection of BL Her stars discovered in the Large Magellanic Cloud (Soszyński et al. 2008). All these variables were identified on the basis of their position in the $P - L$ diagram, which established their BL Her nature beyond doubt. Fig. 7 shows that there is nothing unusual about the light curves of BLG184.7 133264 and BLG189.6 137529. In fact, they are very similar to the light curves of BL Her stars observed in the LMC. This statement can be put on a more quantitative basis with the help of the Fourier decomposition parameters $R_{k1} = A_k/A_1$ and $\phi_{k1} = \phi_k - k\phi_1$, where the A_k and ϕ_k are defined by Eq. 1 or Eq. 2. The values of R_{k1} and ϕ_{k1} for the light curves of BLG184.7 133264 and BLG189.6 137529 are given in Tab. 1. In Fig. 8 these values are compared with the Fourier parameters of the Type II Cepheids of the LMC. Both period-doubled variables are firmly located on the Fourier parameter progressions defined by the LMC pulsators. This is particularly striking in the plot of the ϕ_{31} vs. period, where Type II Cepheids form a very tight, well defined sequence. Based on Figs 6, 7 and 8, we conclude that BLG184.7 133264 and BLG189.6 137529 are perfectly normal BL Her-type variables and, except of the period doubling, they do not differ in any way from other pulsators of this class.

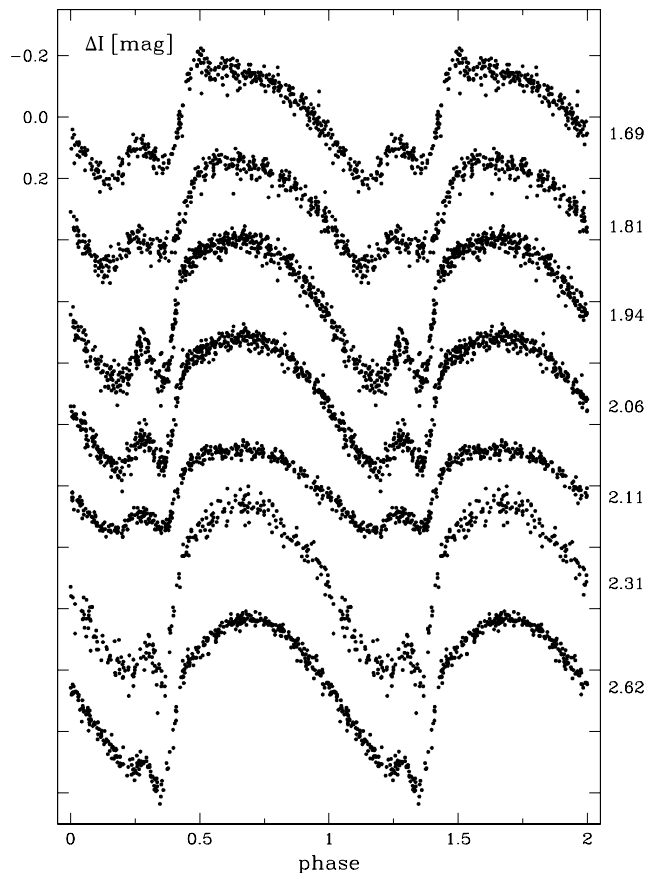


Figure 7. Light curves of selected BL Her stars of the LMC (Soszyński et al. 2008). Numbers at the right side of the plot show periods (in days) of the displayed variables.

3 HYDRODYNAMIC MODELS

The discovery of the first BL Herculis star showing the period doubling motivates a new survey of convective hydrodynamic models including up to date physics. In this Section we report the results of such initial model survey in which our goals are the following: (i) to check whether the period doubling is possible in the convective BL Her models with the fundamental mode period equal to 2.4 d; (ii) to confirm the crucial role of the 3:2 resonance, $3\omega_0 = 2\omega_1$, evident from the earlier radiative models of Buchler & Moskalik (1992); (iii) to model the light curve of the only firm BL Her star showing the period doubling and (iv) to constrain its physical parameters (mass, luminosity, metallicity) based on the comparison of the computed models with observations.

In Section 3.1 we briefly present the convective hydrocodes used in this study and provide the details on the adopted model parameters. Results of the model survey are presented in the following sections, first, the results of extensive linear model survey (Section 3.2), and next, the results of non-linear model computations focused on reproducing the light curve of BLG184.7 133264 (Section 3.3).

3.1 Numerical methods

In all model computations we use the convective pulsation hydrocodes described by Smolec & Moskalik (2008). The

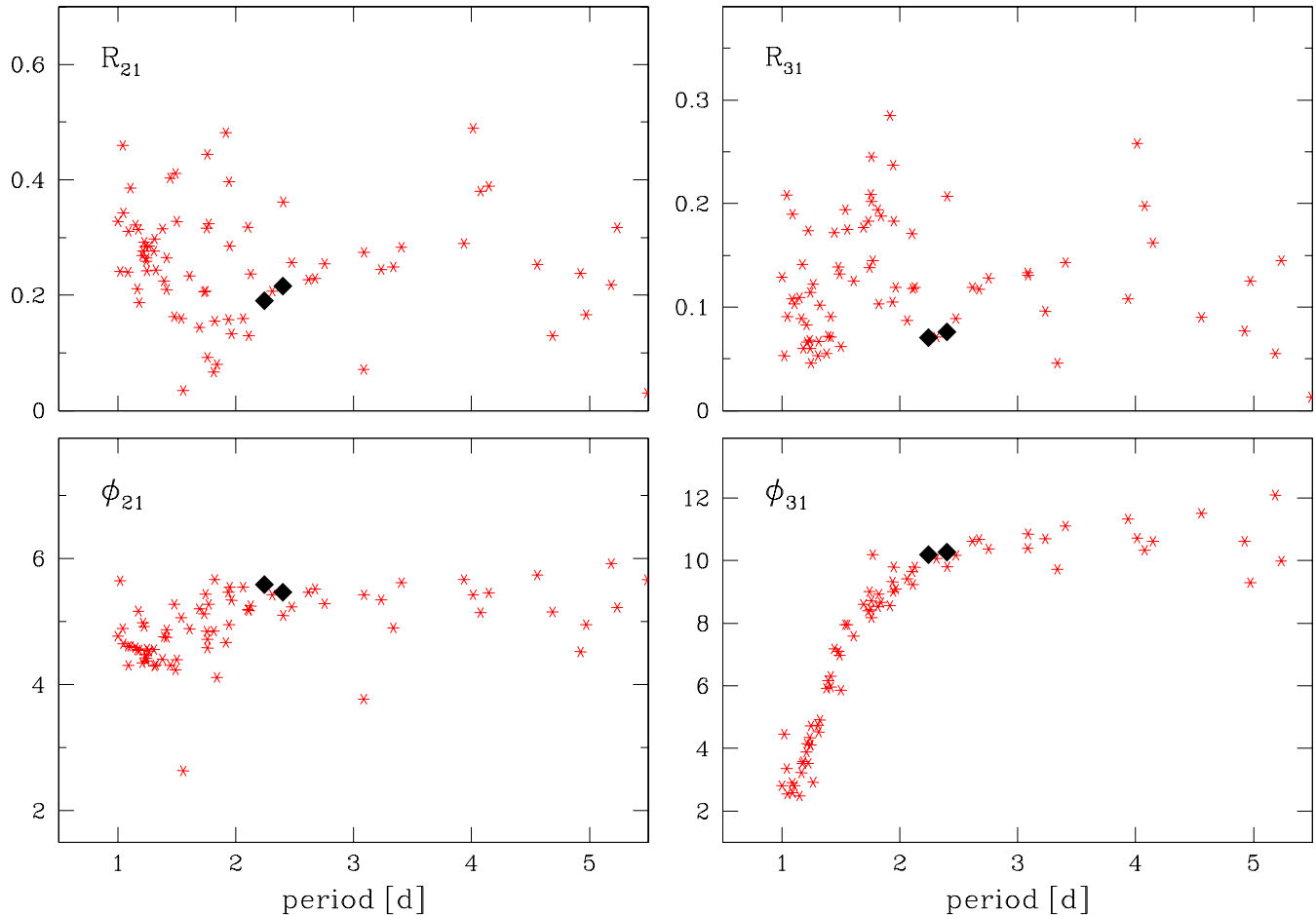


Figure 8. *I*-band Fourier parameter progressions for the Type II Cepheids. Asterisks represent Type II Cepheids of the LMC (Soszyński et al. 2008). BLG184.7 133264 and BLG189.6 137529 are plotted with diamonds. Their ϕ_{31} values are shifted up by 2π .

codes are Lagrangian. Radiative transfer is treated in the diffusion approximation. For the convective energy transfer we use the Kuhfuß (1986) time-dependent model adopted for the use in the pulsation hydrocodes. Kuhfuß model is a simple, one dimensional formulation, with one additional equation describing the generation of the turbulent energy. All equations and details are given in Smolec & Moskalik (2008). The model contains eight order-of-unity scaling parameters. These are the mixing-length parameter, α , and parameters scaling the turbulent fluxes and the terms that drive/damp the turbulent energy, α_p (turbulent pressure), α_m (eddy-viscous dissipation), α_c (convective heat flux), α_t (kinetic turbulent energy flux), α_s (buoyant driving), α_d (turbulent dissipation) and γ_r (radiative cooling). Theory provides no guidance for their values however, some standard values are in use. They result from comparison of a static, time-independent version of the model with the standard mixing-length theory (see Wuchterl & Feuchtinger 1998; Smolec & Moskalik 2008). In practice, values of the parameters are adjusted to get the models that satisfy as many observational constraints as possible. Parameters used in this study are summarised in Table 2. In this initial study (see Section 5) we neglect the effects of turbulent pressure and turbulent overshooting. Set P1 is our basic choice.

Static envelope models were constructed using 180 mass

Table 2. Convective parameters considered in this study. Parameters α_s , α_c , α_d , α_p and γ_r are given in the units of standard values ($\alpha_s = \alpha_c = 1/2\sqrt{2/3}$, $\alpha_d = 8/3\sqrt{2/3}$, $\alpha_p = 2/3$ and $\gamma_r = 2\sqrt{3}$; see Smolec & Moskalik 2008, for details).

set	α	α_m	α_s	α_c	α_d	α_p	α_t	γ_r
P1	1.5	0.25	1.0	1.0	1.0	0.0	0.0	0.0
P2	1.8	0.25	1.0	1.0	1.0	0.0	0.0	0.0
P3	1.5	0.85	1.0	1.0	1.0	0.0	0.0	1.0

shells, extending down to 2×10^6 K, with the fixed temperature ($T_a = 15\,000$ K) in the anchor zone located 70 zones below the surface. Such mesh structure, with large number of zones between the hydrogen ionisation region and the surface, allows for better resolution of the convective zone in the non-linear computations, which becomes very thin during the expansion phases, sweeping inward through the Lagrangian zones of the model.

The static model is perturbed (“kicked”) with the scaled linear velocity eigenvector and time evolution is followed. By default, non-linear model integration is conducted for 1000 pulsation cycles. With typical linear growth rates characterising BL Her stars, on order of 0.1 d^{-1} , the limit cycle

pulsation is reached only after several tenths of pulsation periods.

Non-linear models of BL Her stars, are numerically much more demanding than the models of RR Lyrae stars. Having roughly the same mass, BL Her stars are 2–3 times more luminous. Extended envelope is strongly non-adiabatic and pulsations are rather violent. Consequently artificial viscosity, for which we use the von Neumann and Richtmyer prescription (Richtmyer 1957), turns on in the models. We adopt the following values for the artificial viscosity parameters (see Stellingwerf 1975), $C_q = 4.0$ and a large cut-off parameter $\alpha_{\text{cut}} = 0.1$. Large value of the cut-off parameter (0.1 as compared to 0.01 used by default in the radiative computations, see e.g. Buchler & Moskalik 1992) assures that the artificial viscosity plays a role only in the regions of the strongest velocity gradients, located in a few outermost layers of our models, and consequently does not affect the dynamics of pulsation¹.

In order to compare the models with the OGLE *I*-band light curve of BLG184.7 133264, the bolometric light curve is transformed to the *I*-band by computing the bolometric correction and $(V - I)$ colour at each pulsation phase. To this aim static Kurucz (2005) atmosphere models² are used.

3.2 Linear model survey

In our model survey we consider four values of model masses, $M = 0.50 M_\odot$, $0.55 M_\odot$, $0.60 M_\odot$ and $0.65 M_\odot$. The adopted luminosities are in large range of $90 - 280 L_\odot$. In all our models the hydrogen abundance is fixed, $X = 0.76$, and three different heavy element abundances are considered, $Z = 0.0001$, 0.001 and 0.01 . The OP opacities (Seaton 2005) generated for the solar mixture of Asplund et al. (2004) are used. At the low temperatures they are supplemented with the Alexander & Ferguson (1994) opacity data, which is available for the Grevesse & Noels (1993) mixture³. Parameters of the models are not bounded by the evolutionary constraints. Later, in Section 4, we compare our models with the recent horizontal branch evolutionary tracks.

Results of the linear model survey are shown in the HR diagrams presented in Figs 9 and 10. Fig. 9 which shows the results for $M = 0.55 M_\odot$ and $Z = 0.001$ is more detailed than Fig. 10 in which we show the results for the full grid of considered masses and metallicities. In these models convective parameters of set P1 were used. In both figures the instability strips are shown as shaded areas, light grey for the fundamental mode, and dark grey for the first overtone. Typical width of the instability strip is on order of 1 000 K. First overtone can be unstable only for the lowest luminosities. Thick solid line running across the instability strip is the line of constant fundamental mode period equal to 2.4 d

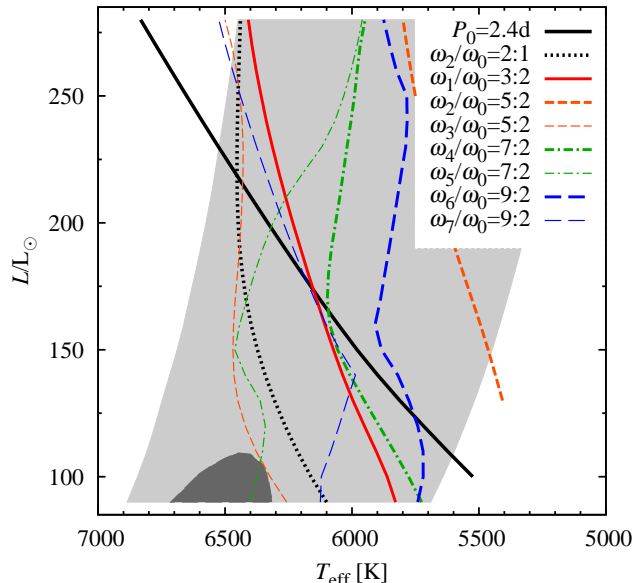


Figure 9. Results of the linear model survey adopting the convective parameters of set P1 (Table 2) and for models with $M = 0.55 M_\odot$ and $Z = 0.001$. The shaded areas show the instability strips for the fundamental mode (light grey) and for the first overtone (dark grey). The thick solid line is the line of constant fundamental mode period, $P_0 = 2.4$ d, and other lines show the loci of various resonances, as indicated in the key. Presented results are based on the interpolation in the extensive grid of linear models with $10 L_\odot$ step in the luminosity and 50 K step in the effective temperature.

(nearly equal to the period of BLG184.7 133264). Thick dotted line (plotted only in Fig. 9) shows the loci of the 2:1 resonance $2\omega_0 = \omega_2$ which is crucial in shaping the bump-progression observed in the light curves of BL Her stars (see Section 1). Other lines show the loci of various half-integer resonances, which are most important in the context of period doubling phenomenon.

In our study we considered all possible half-integer resonances between the fundamental mode and the eight lowest order overtones. Loci of all these resonances are plotted in Fig. 9. Six resonances cross the $P_0 = 2.4$ d line at different luminosities and in principle each of them can be responsible for the period doubling observed in BLG184.7 133264. The most likely candidate is the 3:2 resonance with the first overtone, $3\omega_0 = 2\omega_1$. This resonance was proofed to be responsible for the period doubling in the radiative BL Her models of Buchler & Moskalik (1992). Other resonances however, cannot be excluded *a priori*. Very promising are the high-order resonances with the higher-order overtones, with the sixth and with the seventh order overtones. These modes are special, as they are trapped in the outer envelope, between the surface and the hydrogen ionisation front. Origin and properties of these modes were studied in detail by Buchler et al. (1997) and Buchler & Kolláth (2001). Such modes are characterised by a large growth rates as compared to their not-trapped neighbours. In their study of the half-integer resonances Moskalik & Buchler (1990) showed, that period doubling behaviour is possible if the resonant mode is not damped too strongly (but it does not have to be unstable). Consequently, resonances involving the trapped modes

¹ For the models with the highest L/M ratio artificial viscosity can contribute to the pulsation damping also in the hydrogen-helium ionisation region, but the contribution is small as compared to the damping caused by the turbulent viscosity.

² <http://kurucz.harvard.edu/>

³ The OP and Alexander & Ferguson opacities are stitched together at $\log T = 3.95$, that is in the outer model layers, above partial ionization regions driving the pulsation. Consequently the mismatch in the abundance mixtures does not affect the model behaviour.

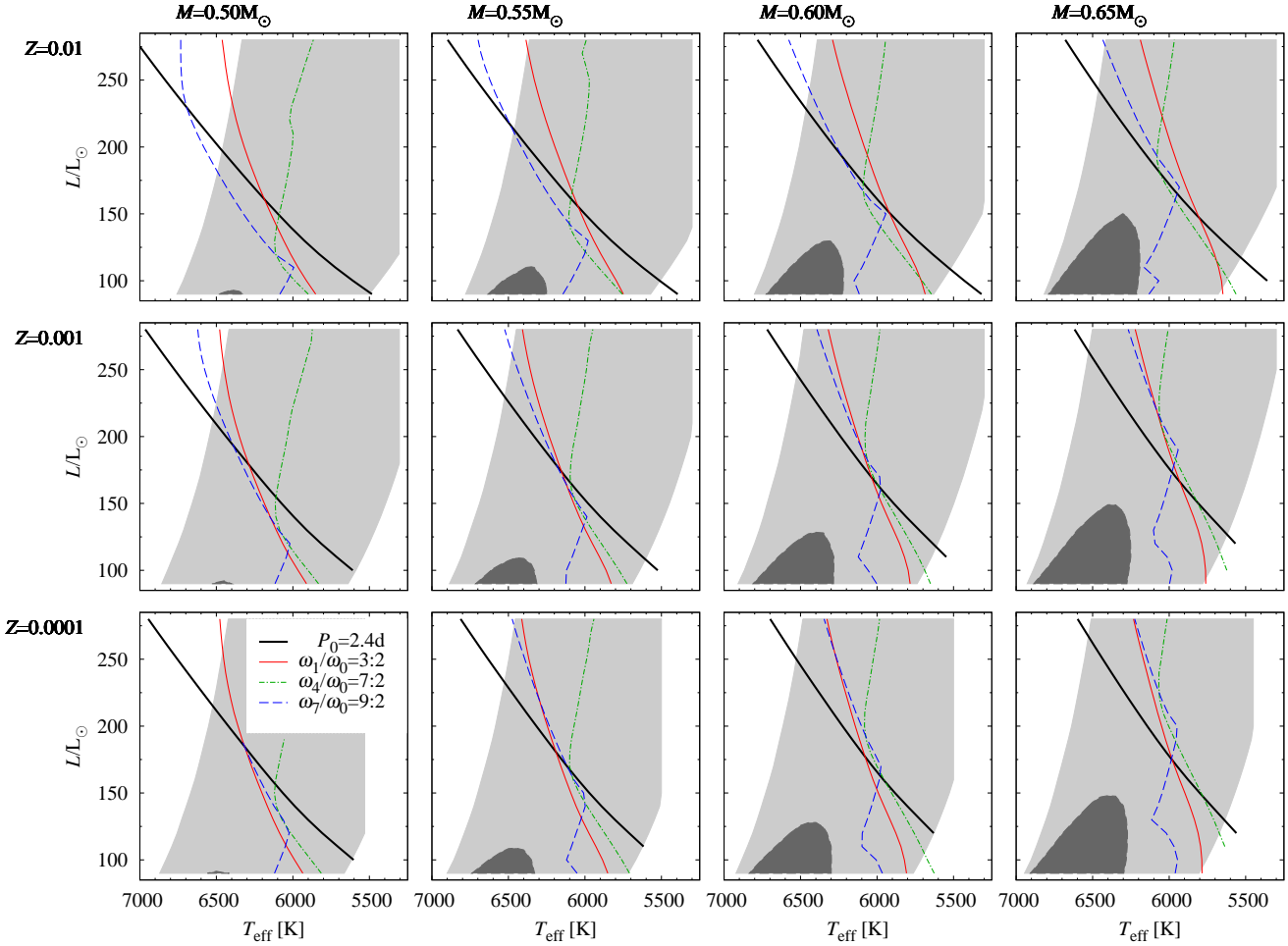


Figure 10. The same as Fig. 9 but for a grid of models with different masses ($0.50 M_{\odot}$, $0.55 M_{\odot}$, $0.60 M_{\odot}$, and $0.65 M_{\odot}$, in consecutive columns), and metallicities (0.01, 0.001, and 0.0001, in consecutive rows). For clarity, the loci of only three half-integer resonances are plotted, as indicated in the key in the bottom, left-most panel.

are also the likely candidates to cause the period doubling. In our models the growth rates of the sixth and seventh overtones are close to zero, but the modes remain stable. In addition the modes undergo the avoided crossing, which may be noticed from the run of resonant lines in Fig. 9 (long-dashed lines). We also note that Kolláth et al. (2011) showed that the period doubling discovered recently in several RR Lyrae stars showing the Blazhko effect (Szabó et al. 2010) is caused by the 9:2 resonance with the ninth order overtone, which is a trapped envelope mode in their models. Also our model computations for the Blazhko RR Lyrae stars (Smolec et al. 2011) confirm the crucial role of this resonance.

Fig. 10 illustrates how the location of the resonance loci vary with mass and metallicity of the models. For clarity only the three half-integer resonances are plotted in the Figure, the 3:2 resonance with the first overtone, $3\omega_0 = 2\omega_1$, the 7:2 resonance with the fourth overtone, $7\omega_0 = 2\omega_4$, and the 9:2 resonance with the seventh overtone (trapped mode), $9\omega_0 = 2\omega_7$. These three resonances cross the $P_0 = 2.4$ d line well within the instability strip for almost all considered combinations of M and Z . Other resonances often fall beyond or close to the edge of the instability strip. It is vis-

ible that changes in the location of resonant lines are rather small, but systematics is clear. Considering e.g. the 3:2 resonance and its crossing with $P_0 = 2.4$ d line, one observe that larger the mass (at fixed Z) lower the luminosity and lower the effective temperature at the crossing. The same tendency is observed with the increasing metallicity (at fixed mass). The largest possible luminosity at the crossing is $L \approx 185 L_{\odot}$ at $T_{\text{eff}} \approx 6316$ K ($M = 0.50 M_{\odot}$, $Z = 0.0001$), while the lowest possible luminosity is $L \approx 147 L_{\odot}$ at $T_{\text{eff}} \approx 5804$ K ($M = 0.65 M_{\odot}$, $Z = 0.01$). We note that model periods depend only weakly on the convective parameters of the models. Sensitivity is larger for the period ratios and thus, also for the location of the resonant lines. The quantitative picture arising from Figs 9 and 10 however, is the same for other sets of convective parameters, in particular for sets P2 and P3 considered in this study.

Linear computations show, that at least several half-integer resonances can play a role in destabilising the fundamental mode and giving rise to the period doubling behaviour in a models with fundamental mode period of 2.4 d. However proximity to the resonance centre and weak damping of the resonant overtone are not sufficient conditions. The non-linear effects which determine the

mode interaction are crucial here and only full amplitude non-linear computations can reveal whether and which resonance can cause the period doubling.

3.3 Non-linear model survey

In this Section we present the results of non-linear model survey aimed to model the light curve of BLG184.7 133264, in particular, to reproduce the period doubling behaviour and to investigate its causes. All model sequences run across the fundamental mode instability strip, along the lines of constant period equal to 2.4 d (Figs 9 and 10). Thirty six model sequences were computed, for all considered values of model masses ($0.50 M_{\odot}$, $0.55 M_{\odot}$, $0.60 M_{\odot}$ and $0.65 M_{\odot}$), model metallicities (0.01, 0.001 and 0.0001) and for the three sets of convective parameters (P1, P2 and P3, Table 2). Individual models in a sequence are specified by the static luminosity, which is changed in the $2 L_{\odot}$ steps. Effective temperature is adjusted to match the $P_0 = 2.4$ d (for considered mass and metallicity). We note that full amplitude non-linear periods may slightly differ from the linear value and in our models are usually longer by up to 3 per cent.

Bolometric light curves are transformed to the I -band (see Section 3.1) and next, are fitted with the Fourier series (equation 2). We also compute the Fourier decomposition parameters of low order, the amplitude ratios, R_{k1} , and phase differences, ϕ_{k1} (see Section 2.3).

Exemplary I -band light curves from model sequence with $M = 0.50 M_{\odot}$ and $Z = 0.01$ (set P1) are shown in Fig. 11. Pulsation period is roughly the same for all these models, $P_0 \approx 2.4$ d. Systematic change of the light-curve shapes is clearly visible. Model with the largest luminosity ($190 L_{\odot}$) has a regular triangular shape almost void of secondary features. As luminosity decreases the secondary features such as bumps, become more and more pronounced. Of great interest is the bump close to the minimum brightness, which is also visible in the light curve of BLG184.7 133264 (Fig. 2), as well as in some other BL Her-type variables (e.g. Fig. 7). Its amplitude increases with the decreasing luminosity. Another bump is visible close to the maximum brightness and is most pronounced for the lowest luminosity models. One may also note a series of wiggles of very low amplitude on the descending branch. It is a numerical effect caused by the lack of resolution in the convective zone which becomes very thin during the expansion phases (close to maximum radius, see also Section 3.1). Period doubling is clearly visible in several models with luminosities in a range $140 - 170 L_{\odot}$.

For other model sequences we observe qualitatively the same picture. In nearly all our model sequences period doubling behaviour is evident for several models. In Section 3.3.1 we focus on the origin of this phenomenon. Later in Section 3.3.2 we focus on the light-curve shapes and search for the best-fitting model for BLG184.7 133264.

3.3.1 Origin of the period doubling

Period doubling is caused by the destabilisation of the fundamental mode by the resonant overtone. The stability of the limit cycle pulsation can be studied using the relaxation technique (Stellingwerf 1974), which shows whether

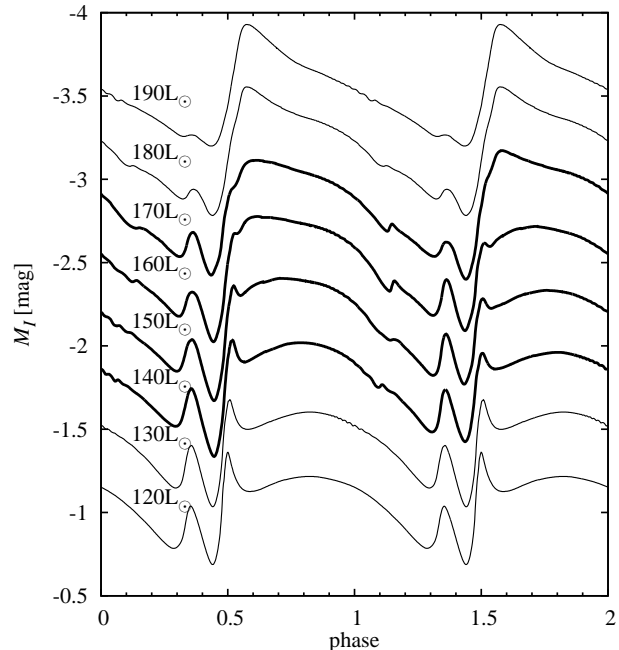


Figure 11. A sample of I -band light curves from the model sequence with $M = 0.50 M_{\odot}$ and $Z = 0.01$ (set P1). For clarity, the consecutive light curves are shifted arbitrarily by 0.3 mag. Each light curve is marked with luminosity value on the left-hand side. Light curves showing the period doubling phenomenon ($140 - 170 L_{\odot}$) are plotted with thick lines.

the non-linear limit cycle is stable or not with respect to the possible perturbation in other (resonant) mode. Such analysis was done by Buchler & Moskalik (1992) for their radiative BL Her models. The period doubling domain they found coincide with the 3:2 resonance centre. Using the relaxation technique they showed that for these models the fundamental mode limit cycle is unstable with respect to the first overtone, pointing to the crucial role played by the resonance.

Unfortunately, the relaxation scheme is not implemented in our convective hydrocodes. Consequently, we are left to judge on the role played by particular half-integer resonance in the computed period doubling behaviour, based on the distance of the model to the resonance centre (mismatch parameter, Δ), which is computed using the linear period ratios. One has to remember that when non-linear results are correlated with the linear properties of the models, the models have to be computed in a consistent way, i.e. using the same numerical mesh and the same input physics (see e.g. Buchler et al. 1990). This is the case of our models.

The existence and strength of the period doubling behaviour in our models is characterised by the amplitude of the sub-harmonic frequency, $B_{1/2}$ (eq. 2). In Fig. 12 $B_{1/2}$ is plotted versus the mismatch parameter for the three half-integer resonances, $3\omega_0 = 2\omega_1$ ($\Delta_{3:2} = \omega_1/\omega_0 - 1.5$) in the top panel, $7\omega_0 = 2\omega_4$ ($\Delta_{7:2} = \omega_4/\omega_0 - 3.5$) in the middle panel, and $9\omega_0 = 2\omega_7$ ($\Delta_{9:2} = \omega_7/\omega_0 - 4.5$) in the bottom panel. Each line in this figure corresponds to one model sequence with given mass and metallicity. All model sequences displayed in Fig. 12 adopt convective parameters of set P1.

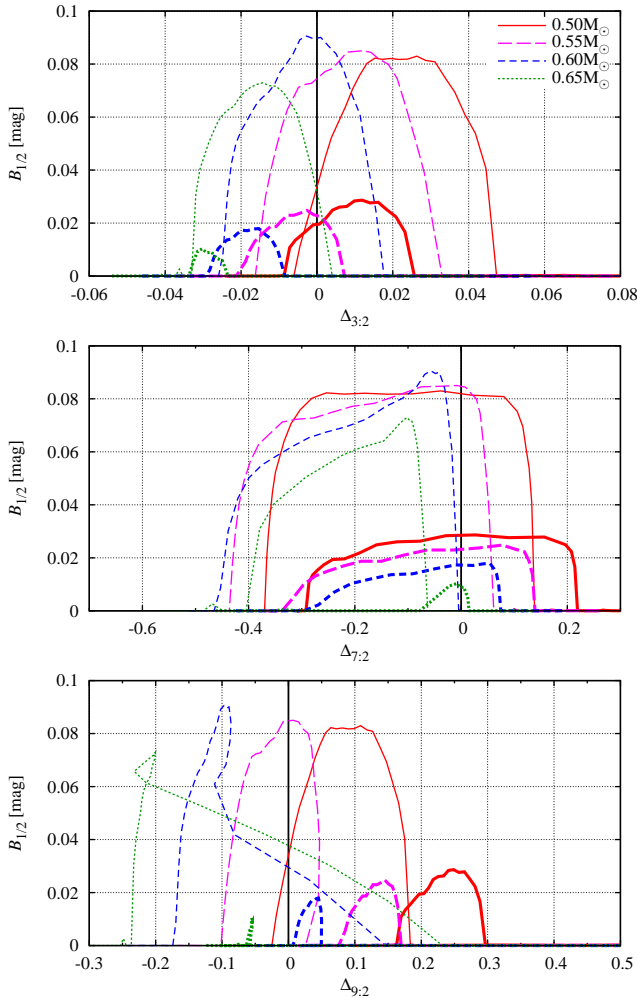


Figure 12. Amplitude of the sub-harmonic frequency component, $B_{1/2}$, plotted versus the mismatch parameters for: (top panel) 3:2 resonance with the first overtone, $\Delta_{3:2} = \omega_1/\omega_0 - 1.5$, (middle panel) 7:2 resonance with the fourth overtone, $\Delta_{7:2} = \omega_4/\omega_0 - 3.5$ and, (bottom panel) 9:2 resonance with the seventh overtone, $\Delta_{9:2} = \omega_7/\omega_0 - 4.5$. Models with different masses are plotted with different line styles as indicated in the key. Metallicity is indicated with the line thickness; the thick lines are for the largest metallicity, $Z = 0.01$ and the thin lines are for the lowest metallicity, $Z = 0.0001$. For clarity, model sequences with $Z = 0.001$ are not shown in the Figure. In all models convective parameters of set P1 (Table 2) were adopted.

For all model sequences we see a single period doubling domain with typical amplitudes of few hundreds of magnitude.

In the top panel of Fig. 12 we clearly see that the period doubling domains always coincide with the $3\omega_0 = 2\omega_1$ resonance centre. In most cases, the resonance centre is located within the period doubling domain. For all models showing the period doubling, the mismatch parameter is always smaller than 0.05 (and is usually much smaller). We note that period doubling domain can be significantly shifted with respect to the resonance centre, as it is e.g. for $M = 0.60 M_\odot$ and $M = 0.65 M_\odot$ ($Z = 0.01$) domains which lie outside the resonance centre. It does not disprove the role played by the resonance however, but can be caused by the

non-linearity and non-adiabaticity of the pulsations (see e.g. Buchler & Moskalik 1992; Smolec 2009a).

The period doubling domains are also close to the $7\omega_0 = 2\omega_4$ resonance centre (middle panel of Fig. 12). In most cases the resonance centre falls somewhere within the period doubling domain. But contrary to the $3\omega_0 = 2\omega_1$ resonance, the range of mismatch parameters is very large, $-0.5 < \Delta_{7:2} < 0.2$. It is highly unlikely that the period doubling is caused by the $7\omega_0 = 2\omega_4$ resonance in the model located as far from the resonance centre as e.g. $|\Delta_{7:2}| > 0.2$ (Moskalik & Buchler 1990).

For the $9\omega_0 = 2\omega_7$ resonance (bottom panel of Fig. 12) conclusions are the same. Most of the period doubling models are located far from the resonance centre. Even the entire period doubling domain can be located as far as $\Delta_{9:2} > 0.15$ (for model sequence with $M = 0.50 M_\odot$ and $Z = 0.01$ – thick solid line in the bottom panel of Fig. 12). Clearly, the 9:2 resonance cannot play any role in these models.

Similar analysis was done for all other possible half-integer resonances which centres fall within the computed model sequences (e.g. for the other three resonances which loci are plotted in Fig. 9), as well as for all model sequences adopting the convective parameters of sets P2 and P3. Only for the 3:2 resonance the mismatch parameter is very small ($|\Delta_{3:2}| < 0.05$) for all the models that show the period doubling. It clearly indicates that the 3:2 resonance plays a key role in causing the phenomenon. The question whether other resonances can play an additional role for some particular models, for which respective mismatch parameter is also close to 0, cannot be answered beyond doubt. It seems however, that this is not the case. The period doubling domains as depicted in Fig. 12 through the amplitude of the sub-harmonic frequency, $B_{1/2}$, seem to be void of features correlated with the location of the centres of the other half-integer resonances (see also Fig. 13). The crucial role of the 3:2 resonance in causing the period doubling behaviour in BL Her type models is also supported by the earlier analysis of radiative models by Buchler & Moskalik (1992). Using the relaxation technique Buchler & Moskalik (1992) proofed the key role of the 3:2 resonance.

In our opinion, the presented results leave no doubt that the 3:2 resonance with the first overtone is responsible for the period doubling in the hydrodynamic models and first of all in BLG184.7133264.

3.3.2 The best model for BLG184.7133264

In this Section we compare the computed model light curves with the light curve of BLG184.7133264 (Fig. 2). Our comparison is based on the low-order Fourier decomposition parameters, the amplitudes, A_1 and $B_{1/2}$, the amplitude ratio, R_{21} , and the phase difference, ϕ_{21} . Higher order parameters are modelled less accurately with the hydrocodes and are not used below. We note that physical parameters of all our models were adjusted to match the linear fundamental mode period of 2.4 d with typical accuracy larger than 0.01 d. Non-linear periods may differ only very slightly. These periods are close enough to the period of BLG184.7133264 and thus allow the direct comparison of the Fourier parameters which is done in Fig. 13 (A_1 versus $B_{1/2}$) and in Fig. 14 (ϕ_{21} versus R_{21}). In these figures we show the results for all the computed models, for the full grid of model

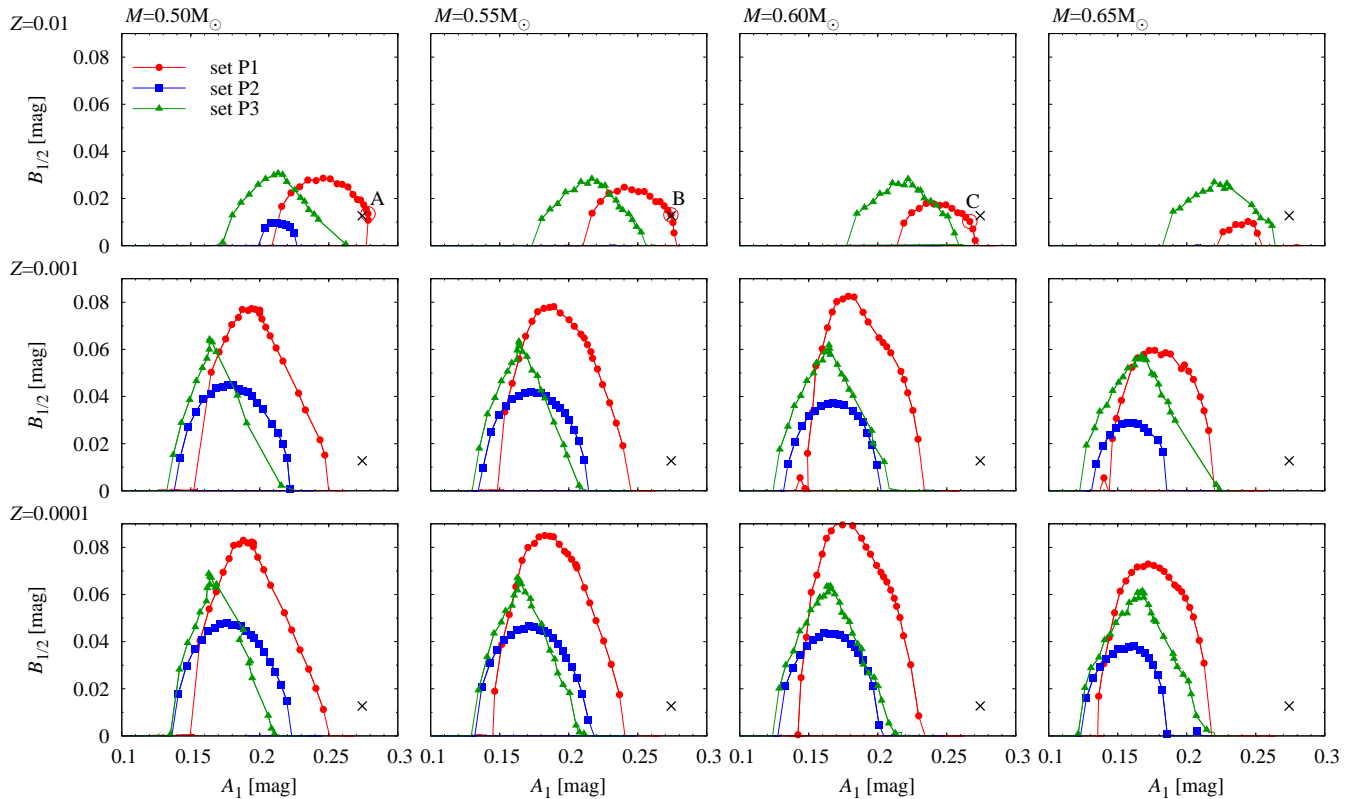


Figure 13. Amplitude of the sub-harmonic frequency component, $B_{1/2}$, plotted versus the amplitude, A_1 , for the full grid of the computed non-linear models. Different sets of convective parameters (Table 2) were used in the computations, as indicated in the key in the top, left-most panel. Cross shows the amplitudes of BLG184.7 133264 (see Section 2). The best matching models of set P1, A ($M = 0.50 M_{\odot}$, $Z = 0.01$), B ($M = 0.55 M_{\odot}$, $Z = 0.01$) and C ($M = 0.60 M_{\odot}$, $Z = 0.01$), are encircled and labelled.

masses ($0.50 M_{\odot}$, $0.55 M_{\odot}$, $0.60 M_{\odot}$ and $0.65 M_{\odot}$, consecutive columns of Figs 13 and 14) and model metallicities (0.01, 0.001, and 0.0001, consecutive rows of Figs 13 and 14). Model sequences adopting different sets of convective parameters are plotted with different symbols, circles (set P1), squares (set P2) and triangles (set P3). Filled symbols correspond to the models showing the period-doubling behaviour, while the models represented by open symbols show no sign of alternations. Only the former models are shown in Fig. 13. By default, the consecutive models in each model sequence differ by $2L_{\odot}$. Sometimes the difference is larger, as some models could not be converged to the limit cycle due to numerical problems (this is true particularly for set P3). Cross in the figures shows the parameters of BLG184.7 133264 (Tab. 1).

To find the best matching model for BLG184.7 133264 we focus on the model amplitudes (Fig. 13), the pulsation amplitude, A_1 , and the amplitude of period doubling, $B_{1/2}$. One could choose the Fourier phases instead (ϕ_{21} and ϕ_{31}), which little depend on the pulsation amplitudes and are also not so sensitive to the values of convective parameters (Smolec 2009b). We note however, that one of the known problems in modelling the light curves with pulsation hydrocodes is that computed Fourier phases are systematically different from the observed phases. The problem was studied in more detail in the RR Lyrae stars (e.g. Dorfi & Feuchtinger 1999; Kovács & Kanbur 1998; Feuchtinger 1999). It was also encountered in the ra-

diative and convective models of classical Cepheids (e.g. Moskalik, Buchler & Marom 1992; Smolec 2009b) and in radiative models of BL Her stars (Moskalik & Buchler 1993a). Origin of the discrepancy is not clear, although the very simplified treatment of the radiation transfer in the subphotospheric layers of all current hydrocodes is the most likely culprit (Dorfi & Feuchtinger 1999).

Consequently we choose to focus on the amplitudes first, even though they depend on the convective parameters of the models stronger, and in the next step, we compare the Fourier phases and amplitude ratios.

In Fig. 13 we observe that in almost all model sequences the period doubling domain is present. Only for three model sequences, all with the largest considered metallicity ($Z = 0.01$, and $M = 0.55 - 0.65 M_{\odot}$), and adopting convective parameters of set P2, period doubling is not present. The other striking feature visible in Fig. 13 are large amplitudes of the period doubling as compared to BLG184.7 133264 and, at the same time, significantly lower pulsation amplitudes, A_1 . The systematics is clear. Lower the mass and higher the metallicity of the models, higher the pulsation amplitude and lower the amplitude of period doubling. Only for the largest metallicity ($Z = 0.01$) we can match the pulsation amplitude of BLG184.7 133264 (for sets P1 and P3). Also for the most metal rich model sequences the amplitude of period doubling is comparable to what we observe in BLG184.7 133264. For lower metallicity models ($Z = 0.001$ and $Z = 0.0001$) the period doubling amplitude

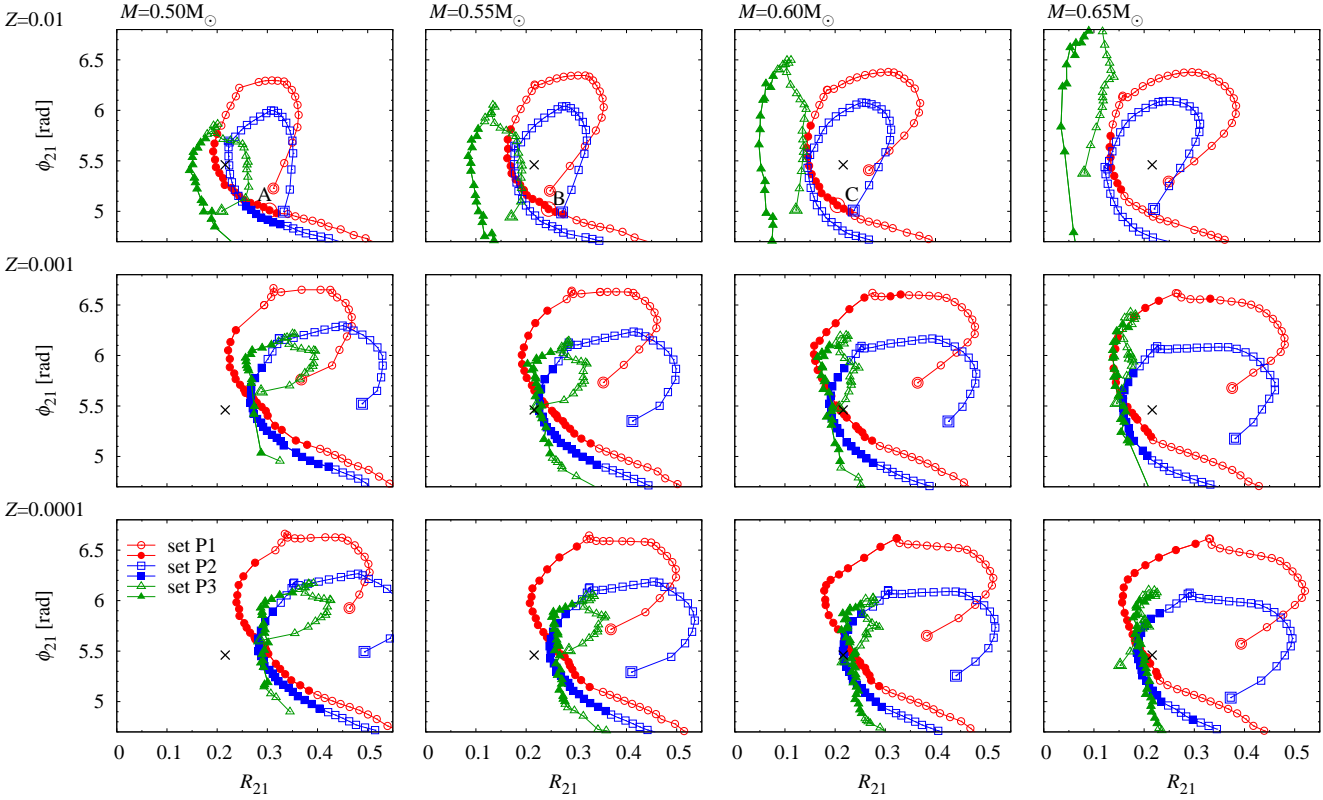


Figure 14. The phase difference, ϕ_{21} , plotted versus the amplitude ratio, R_{21} , for the full grid of the computed non-linear models. Different sets of convective parameters (Table 2) were used in the computations, as indicated in the key in the bottom, left-most panel. Filled symbols correspond to the models showing the period doubling. Crosses represent the Fourier parameters of BLG184.7 133264 (see Table 1). The best matching models of set P1, A, B and C, are encircled and labelled.

is much higher through the whole period doubling domain and matches the amplitude of BLG184.7 133264 only at the domain edges. The large amplitude of period doubling in our models and rather wide range of luminosities over which period doubling domains extend (typically $30 - 40 L_{\odot}$) is somewhat surprising. This suggests that the period doubling should be a rather common feature of BL Her stars with periods around 2.4 d, which is not the case. We will address this problem later in Section 5.

The above analysis of model amplitudes points that BLG184.7 133264 should be of high metallicity. Then, we can simultaneously match its pulsation amplitude and the amplitude of period doubling. This is a likely possibility, as many BL Her stars have high metallicities (see discussion in Section 5). However, one has to remember that model amplitudes depend on the convective parameters adopted in the computations, in particular on the mixing length and on the eddy-viscosity parameter. Comparison of the model results for sets P1 and P2 reveals the effect of changing the mixing length parameter (while keeping all other convective parameters fixed). Mixing length is equal to 1.5 in our basic set P1 and is larger in set P2 ($\alpha = 1.8$). The effect is clear, by increasing the mixing length the pulsation amplitude decreases as well as the amplitude of period doubling (which vanish for $Z = 0.01$ and three largest considered masses, Fig. 13). It seems that one can match the pulsation amplitude of BLG184.7 133264 also for lower metallicities by the decrease of the mixing length below the value adopted in set

P1 ($\alpha = 1.5$). However at the same time the amplitude of period doubling, which is already very large, would increase even more. Also values of the mixing length below 1.5 seem too small, typical values used in model computations being around 1.5–1.8. Recent numerical simulations point to even larger values (Trampedach & Stein 2011).

Mixing length parameter is usually fixed in model computations and it is the eddy viscosity parameter, which is commonly used to adjust the pulsation amplitudes in the convective models. It regulates the amount of viscous dissipation in the model and is a physically motivated counterpart of the artificial viscosity in the radiative models. Pulsation amplitudes of RR Lyrae and Cepheid models clearly depend on that parameter (see e.g. Smolec 2009b). Lower the eddy-viscous dissipation larger the pulsation amplitude. Also the existence and the amplitude of the period doubling computed in the convective RR Lyrae models by Kolláth et al. (2011) depend on the eddy viscosity parameter. Again, lower the eddy-viscous dissipation larger the amplitude of the period doubling in case of the RR Lyrae models. To match the pulsation amplitude of BLG184.7 133264 for metallicities lower than $Z = 0.01$ one has to decrease the eddy viscosity, which will also increase the amplitude of period doubling.

To test the effect of decreasing the eddy-viscosity parameter we have computed two additional model sequences, both with $M = 0.55 M_{\odot}$ and $Z = 0.0001$, and with eddy-viscosity parameter equal to $\alpha_m = 0.20$ and $\alpha_m = 0.15$. The

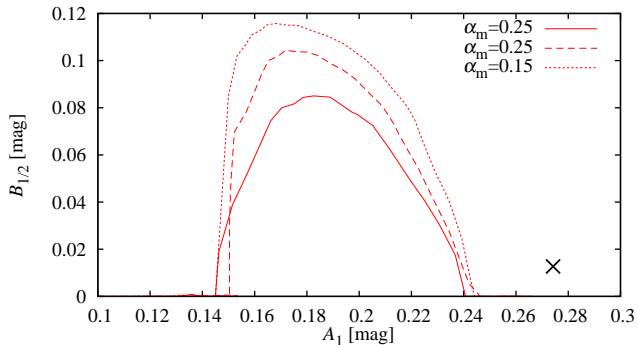


Figure 15. Amplitude of the sub-harmonic frequency component, $B_{1/2}$, plotted versus the amplitude, A_1 , for the three model sequences, all with $M = 0.55 M_{\odot}$ and $Z = 0.0001$, adopting different values of the eddy viscosity parameter: $\alpha_m = 0.25$ (solid line), $\alpha_m = 0.20$ (dashed line) and $\alpha_m = 0.15$ (dotted line). All other parameters of the turbulent convection model are the same as in set P1.

results are shown in Fig. 15 in which $B_{1/2}$ is plotted against A_1 for models of set P1 (solid line, $\alpha_m = 0.25$) and for two additional model sequences, with eddy-viscosity parameter decreased to 0.20 (dashed lines) and 0.15 (dotted line). We note that further decrease of eddy viscosity is not easy. Already with $\alpha_m = 0.20$ pulsation become very violent and we start to face the convergence difficulties. It is clear that amplitude of alternations strongly increase with the decreasing eddy viscosity parameter. However pulsation amplitude increased only very weakly – much too small to match the amplitude of BLG184.7 133264.

Changes of the other convective parameters also affect the pulsation amplitudes which is usually compensated by the change of the eddy viscosity parameter. This is what we have done in set P3, in which we consider the radiative cooling of the convective elements. Inclusion of radiative cooling makes the convection less efficient. Consequently the pulsation amplitudes increase which has to be compensated with the larger value of the eddy viscosity parameter. For the model sequences adopting convective parameters of set P3 we get the period doubling amplitudes higher than for set P2 and similar to that of set P1. The pulsation amplitudes, A_1 , are similar as in set P2. Set P3 is interesting because it leads to significantly different light curve shapes than sets P1 and P2, which we discuss in the next paragraphs.

Based on the model amplitudes we select three models, which match the amplitudes of BLG184.7 133264, for the further, more detailed comparison. The models, A, B and C, are encircled and labelled in Fig. 13. All models adopt convective parameters of set P1, have $Z = 0.01$ and differ in mass ($0.50 M_{\odot}$ for model A, $0.55 M_{\odot}$ for model B and $0.60 M_{\odot}$ for model C). Physical parameters of these models are collected in the upper section of Table 3. Before discussing these models in more detail, we turn into the analysis of the low order Fourier decomposition parameters, the R_{21} amplitude ratio and the ϕ_{21} phase difference. In Fig. 14 the two quantities are plotted for the full grid of the computed models. The range of variation of R_{21} and ϕ_{21} is very large for the considered models all of which have the same pulsation period (≈ 2.4 d). Relation between the two Fourier parameters is very similar for sets P1 and P2, which

differ in the value of the mixing length only, and is significantly different for set P3 in which the effects of radiative losses are turned on. The period doubling domains (filled symbols in Fig. 14) extend over a large range of Fourier phase, ϕ_{21} . There are period doubling models with Fourier phase below 5.0, as well as with Fourier phase well above 6.5. Consequently in all our model sequences we can point the model which shows the period doubling and for which ϕ_{21} matches the value of BLG184.7 133264. For the amplitude ratio we observe that period doubling domains extend around the minimum of R_{21} in the given model sequence. The simultaneous match of the BLG184.7 133264 values of R_{21} and ϕ_{21} (cross in Fig. 14) is possible for several model sequences, which are located along the diagonal in the mass-metallicity plane displayed in Fig. 14. The best match for the lowest metallicity sequences ($Z = 0.0001$) is possible for the highest masses ($0.60 M_{\odot}$ and $0.65 M_{\odot}$). For intermediate metallicity ($Z = 0.001$) we get the best match for the intermediate masses ($0.55 M_{\odot}$ and $0.60 M_{\odot}$), and for the highest metallicity ($Z = 0.01$) we get the best match for the lowest masses ($0.50 M_{\odot}$).

Although for several models we can get an almost exact match between the observed and model values of both R_{21} and ϕ_{21} parameters, only for the highest metallicity models we can match the amplitudes of BLG184.7 133264. For lower metallicities ($Z = 0.001$ and $Z = 0.0001$) the pulsation amplitudes are lower than observed and the amplitudes of alternations are much higher (see Fig. 13).

The three models of $Z = 0.01$, A, B and C, which match the amplitudes of BLG184.7 133264 best, are also labelled in Fig. 14. These models are relatively distant from the cross showing the location of BLG184.7 133264 and for the lower luminosity models from the same model sequence the R_{21} and ϕ_{21} can be matched much better. Still the agreement for models A, B and C is reasonable, as quantitative comparison presented in the lower section of Table 3 shows. For model C the R_{21} amplitude ratio is lower than observed by only 5 per cent and the ϕ_{21} phase difference is lower by 0.41 rad. The agreement is similar for model B and slightly worse for model A for which the amplitude ratio is significantly different than observed. In Table 3 we also provide the comparison for higher order Fourier parameters, R_{31} and ϕ_{31} . The differences are very large. Model values of R_{31} are much larger than observed, even for the best model C, by as much as 85 per cent. For ϕ_{31} the lack of agreement is also remarkable, the model phases being much lower than observed. Detailed analysis of all our models points that although we can easily find models for which two Fourier parameters (e.g. both phases) simultaneously match the observed values, the simultaneous match of all low order Fourier parameters (amplitudes, amplitude ratios and phases) is not possible.

In Fig. 16 we directly compare the *I*-band light curves of BLG184.7 133264 (Fig. 2) and the three selected models A, B and C. The model light curves were shifted vertically in order to match the maximum brightness of BLG184.7 133264, and shifted in phase, so the ascending branches of the light curves overlap. The overall light curve shape of BLG184.7 133264 is nicely reproduced by all three models, but several discrepancies are apparent. In the observed light curve, after the pronounced shoulder on the ascending branch the light raise becomes less steep. The observed light curve is rounded at the maximum light. The shoulder is also visible in the

Table 3. Parameters of the best matching models for BLG184.7 133264. In the top section of the Table physical parameters are provided and in the bottom section of the Table the Fourier decomposition parameters are given. The differences with respect to BLG184.7 133264 (model–star) are given in the parentheses (relative differences for amplitudes and amplitude ratios).

model:	A	B	C
<i>physical parameters</i>			
M/M_{\odot}	0.50	0.55	0.60
L/L_{\odot}	168.0	176.0	184.0
T_{eff} [K]	6241.6	6201.4	6167.2
<i>Fourier parameters</i>			
A_1	0.2784 (+1.5%)	0.2740 (−0.1%)	0.2667 (−2.7%)
$B_{1/2}$	0.0135 (+6.5%)	0.0131 (+2.8%)	0.0103 (−19.1%)
R_{21}	0.304 (+40.7%)	0.245 (+13.4%)	0.205 (−5.1%)
ϕ_{21}	5.010 (−0.451)	5.022 (−0.439)	5.060 (−0.401)
R_{31}	0.236 (+211%)	0.185 (+143%)	0.140 (+84%)
ϕ_{31}	3.376 (−0.618)	3.054 (−0.940)	2.709 (−1.285)

models however, the ascending branch is steep all the time till the maximum brightness which consequently occurs at earlier phases in the models. The light fall also begins earlier and as a result the overall width of the light curve is slightly smaller in the models. At brightness minimum the pronounced bump is clearly visible in both the observations and in the models. Its location is well reproduced by the models, but its amplitude in the models is much higher. The changing character of the brightness minima around the bump during the alternations (each second minimum after the bump is deeper) is qualitatively reproduced by the models. Clearly we get the best agreement for model C, which is also confirmed by more quantitative comparison (Table 3), but the agreement for the other two models is reasonable, as well.

The discrepancies between the model and the observed light curves are not very serious. They concern only the more subtle features of the light curve, like the detailed shape of the brightness maximum or minimum. Such discrepancies are reflected predominantly in the higher order Fourier parameters. Accurate modeling of these higher order Fourier terms is a very challenging problem, though. Of particular importance is the treatment of radiative transfer in the outer zones of the model and the transformation of the bolometric light curve to the *I*-band light curve. These are both treated in a very approximate way in our code (see Section 3.1). Therefore, we do not expect that the models will satisfactorily reproduce all details of the observed light curves. This is a well known deficiency, common to all hydrodynamic models of large amplitude radial pulsators (e.g., Kovács & Kanbur 1998).

Comparison of the observed and model light curves for BLG184.7 133264 point that the star should be of relatively high metallicity ($Z \approx 0.01$) and its mass should be lower than $0.60 M_{\odot}$. Its luminosity should be large around $170 - 180 L_{\odot}$. In the next Section we confront these parameters with the results of recent horizontal branch evolutionary models.

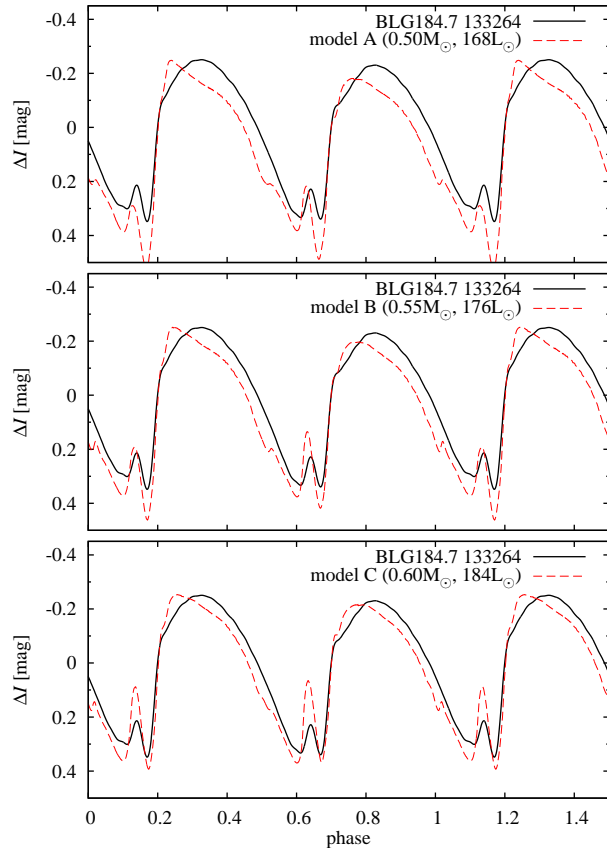


Figure 16. Comparison of the observed *I*-band light curve of BLG184.7 133264 (solid line) with the best matching models of $0.50 M_{\odot}$ (top panel), $0.55 M_{\odot}$ (middle panel) and $0.60 M_{\odot}$ (bottom panel). The model light curves were shifted vertically to match the maximum brightness of BLG184.7 133264 and shifted in phase so the ascending branch of the models and observed light curve overlap.

4 COMPARISON WITH THE EVOLUTIONARY TRACKS

The evolutionary status of BL Her stars was discussed in a series of papers by Gingold (see Gingold 1985, for a summary). Since then, several groups published the horizontal branch (HB) evolutionary tracks for extensive grid of models covering a large range of masses and chemical compositions. These include e.g. Y^2 tracks by Yi et al. (1997), Padova tracks by Girardi et al. (2000), the BaSTI tracks by Pietrinferni et al. (2006) and the Dartmouth tracks by Dotter et al. (2008). Below we briefly review the Gingold's results and compare them with the outcome of more recent evolutionary computations. To this aim we use the BaSTI and Dartmouth tracks. Based on the location of the BL Her instability strip in the HR diagram we conclude on the possible masses of BL Her stars as predicted by the evolution theory. Finally, a comparison with the parameters of our best fitting models for BLG184.7 133264 (Section 3.3.2) is done.

Modelling of the post-main sequence evolution of the low-mass stars is particularly difficult (see e.g. Chiosi et al. 1992). During the evolution along the red giant branch (RGB) these stars develop a degenerate helium core. Then

mass of the core reaches a critical value the runaway helium burning (so called helium flash) is initiated. This violent and rapid phase of the evolution, accompanied by a substantial mass-loss, cannot be followed with the current evolutionary codes. Instead the evolution is restarted at the Zero-Age Horizontal Branch (ZAHB), at much larger effective temperatures. Progenitors of the BL Her stars start their evolution at the blue side of the ZAHB, far beyond the blue edge of the instability strip. During the core helium burning, which is a relatively long phase of the evolution, they remain close to the ZAHB. As the helium becomes gradually depleted in the core, the evolution becomes faster and star moves towards the red, crossing the instability strip and thus, becoming a BL Her variable. According to Gingold evolutionary computations two scenarios are possible, which depend mostly on the mass of the envelope (see fig. 1 in Gingold 1985). In the first scenario, the star crosses the instability strip once and evolves away up along the asymptotic giant branch (AGB). This is the scenario which one can also see in Figs 17 and 18. In the second scenario, so called ‘bluenose’ is possible. Due to the structure changes between the helium and hydrogen burning shells, after approaching the AGB the evolution is directed to the blue and then, back towards the AGB. Two additional crossings of the instability strip are then possible before the star finally climbs-up along the AGB. In both scenarios the star can enter the instability strip again, during the post-AGB evolution (while executing the thermal pulses), becoming a W Vir or RV Tau-type variable.

Both types of tracks can be found in the more recent evolutionary computations, however, the ‘bluenose’ behaviour is very rare. It occurs in a narrow range of masses, and only for larger than solar metallicities (BaSTI, Dartmouth) and in addition in models assuming a large enhancement of the α -elements ($[\alpha/\text{Fe}] > +0.6$, Dartmouth). We do not discuss this scenario in the following.

The recent evolutionary tracks are displayed in Figs 17 (BaSTI) and 18 (Dartmouth). In these figures the edges of the instability strip are marked with solid, vertically running lines. The grey-shaded area in between corresponds to the BL Her pulsation domain with fundamental mode periods between 1 d (lower boundary of the shaded area) and 4 d (upper boundary of the shaded area)⁴. Below that region the RR Lyrae instability strip extends. The following discussion is based on the BaSTI tracks. In the three panels of Fig. 17 we have plotted the evolutionary tracks for three different metallicities, $Z = 0.0001$ in the left-hand panel, $Z = 0.001$ in the middle panel and $Z = 0.01$ in the right-hand panel. Several evolutionary tracks for different model masses are plotted. It is clearly visible that for a given metallicity, the masses of models which can enter the BL Her domain during the evolution are restricted. First, consider the lowest metallicity models ($Z = 0.0001$, left-hand panel of Fig. 17). Model with the largest mass displayed in the figure ($M = 0.65 M_{\odot}$) cross the BL Her domain at its lower part at $L < 80 L_{\odot}$. Lower the model mass, higher the luminosity at the crossing with the BL Her domain. The models with $M \geq 0.54 M_{\odot}$ enter the instability strip. For lower masses, crossing with

the instability strip occurs at larger luminosities, above the BL Her domain, or does not occur at all (evolution along almost vertical tracks or even to the blue). As the metallicity is increased evolutionary tracks for models of a given mass (their pre-AGB part) shift towards the red and bend towards the lower luminosities. Consequently the less massive models can enter the BL Her domain from the top. On the other hand, the tracks for most massive models leave the BL Her domain running below it. For $Z = 0.001$ (middle panel of Fig. 17) the tracks for models with $0.52 M_{\odot} \leq M \leq 0.60 M_{\odot}$ cross the instability strip and for $Z = 0.01$ (right-hand panel of Fig. 17) the range of possible masses is even smaller, $0.50 M_{\odot} \leq M \leq 0.54 M_{\odot}$. All tracks with $M > 0.54 M_{\odot}$ run below the BL Her domain or even start beyond the red edge of the instability strip ($0.60 M_{\odot}$).

Qualitatively the same scenario is evident from the analysis of the Dartmouth evolutionary tracks plotted in Fig. 18. The one-to-one comparison with the BaSTI tracks is difficult, because the Dartmouth tracks were computed for specific values of $[\text{Fe}/\text{H}]$, which do not correspond to the Z values adopted in the BaSTI tracks. In Fig. 18 we have also plotted additional set of evolutionary tracks for models adopting slightly enhanced abundance of the α -elements. Detailed list of the elements with their abundances can be found in table 2 of Dotter et al. (2008). Their table 3 provides the corresponding metallicity values, Z , which we also provide in Fig. 18. Just as for the BaSTI tracks we observe that lower the metallicity, larger the possible masses (and larger their range) of models crossing the BL Her domain during the evolution. The main effect of increasing the abundance of the α -elements is shift of the tracks towards the lower luminosities and slightly lower effective temperatures. Consequently, for the models with increased abundance of the α elements the range of possible masses that allow for crossing the BL Her domain (at given Z) shifts towards slightly smaller mass values.

Presented results are also in qualitative agreement with the Y^2 (Yi et al. 1997) evolutionary models as well as with the Padova (Girardi et al. 2000) HB tracks (for $M \geq 0.55 M_{\odot}$; tracks assuming lower M are not present in the Padova database).

As discussed above, the evolution theory put constraints on the possible masses of the BL Her stars, which depend on the metallicity. Larger the metallicity, lower the possible masses of the BL Her stars. This has severe consequences for our best matching models for BLG184.7 133264 discussed in Section 3.3.2, A, B and C, all of which have $Z = 0.01$. The models are shown with different symbols in Figs 17 and 18. Comparison is straightforward for the BaSTI tracks, as these were computed also for $Z = 0.01$, and is done in the right-hand panel of Fig. 17. We clearly see that models B ($M = 0.55 M_{\odot}$) and C ($M = 0.60 M_{\odot}$) cannot be matched by the respective evolutionary tracks. Tracks for these masses run below the BL Her domain. To the contrary, model A is in excellent agreement with the evolutionary computations, the track for model of $0.50 M_{\odot}$ nearly crosses the square representing model A in the Figure. The one-to-one comparison with the Dartmouth tracks is somewhat difficult as metallicity of our best models, $Z = 0.01$, falls in between $[\text{Fe}/\text{H}] = 0.0$ and $[\text{Fe}/\text{H}] = -0.5$ for which the Dartmouth tracks were computed. Consequently, we have plotted the models in both the middle ($Z \approx 0.0054$) and

⁴ Location of the instability strip is approximate. It was computed assuming $M = 0.55 M_{\odot}$, $Z = 0.001$ and convective parameters of set P1.

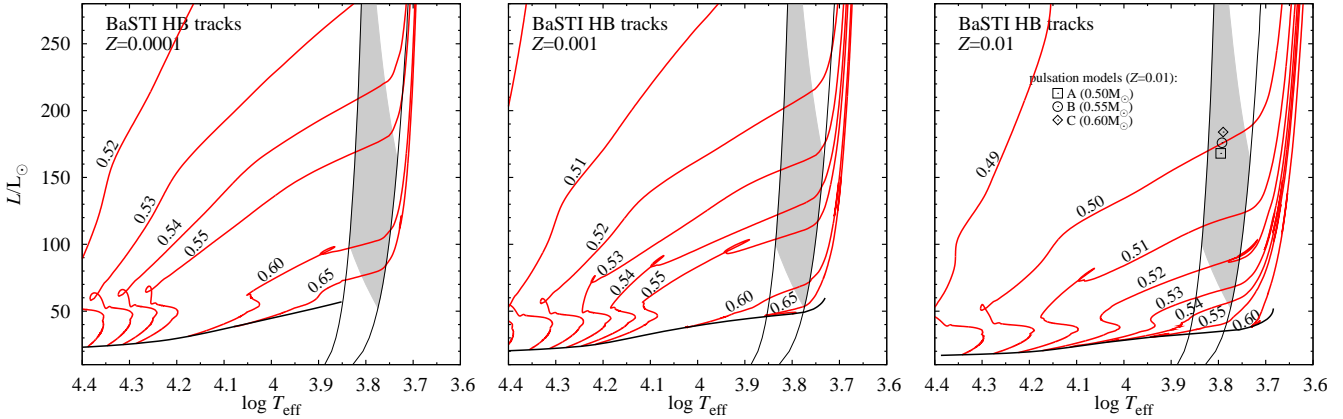


Figure 17. The BaSTI (Pietrinferni et al. 2006) horizontal branch evolutionary tracks for three values of model’s metallicity, $Z = 0.0001$ in the left-hand panel, $Z = 0.001$ in the middle panel and $Z = 0.01$ in the right-hand panel. Evolutionary tracks start at the ZAHB, which is marked with the solid, horizontally running line. Each track is labelled with the corresponding model mass. Over-plotted are the edges of the instability strip, with the shaded area indicating the BL Her domain, with fundamental mode periods between 1 d (lower boundary of the shaded area) and 4 d (upper boundary of the shaded area).

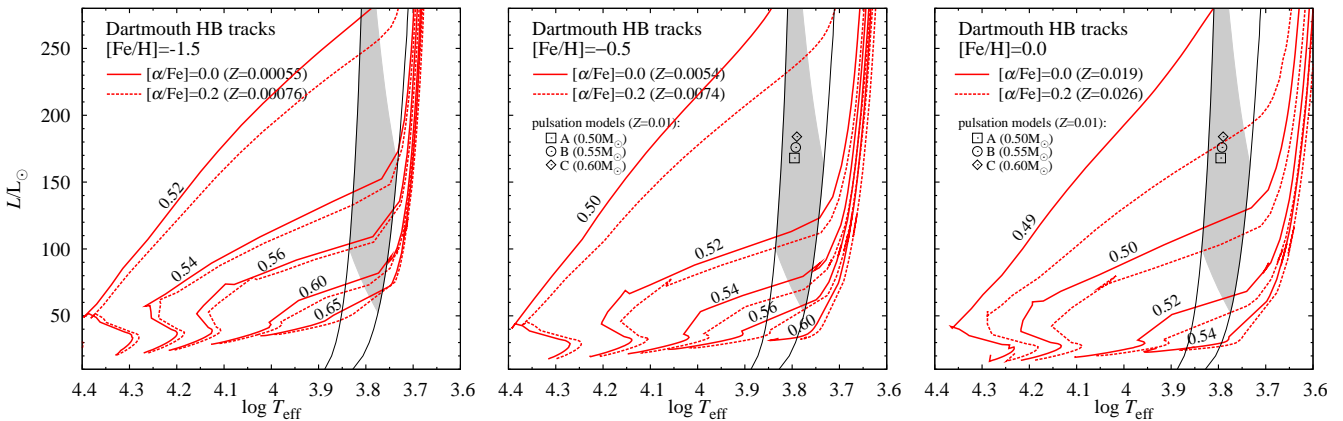


Figure 18. The Dartmouth (Dotter et al. 2008) horizontal branch evolutionary tracks for three values of model’s iron abundance, $[\text{Fe}/\text{H}] = -1.5$ in the left-hand panel, $[\text{Fe}/\text{H}] = -0.5$ in the middle panel and $[\text{Fe}/\text{H}] = 0.0$ in the right-hand panel. The evolutionary tracks are labelled with the corresponding model mass. In each panel we also plotted additional set of evolutionary tracks for models assuming enhanced abundance of the α -elements, $[\alpha/\text{Fe}] = +0.2$ (dashed lines). Over-plotted are the edges of the instability strip, with the shaded area indicating the BL Her domain, with fundamental mode periods between 1 d (lower boundary of the shaded area) and 4 d (upper boundary of the shaded area).

right-hand panel ($Z \approx 0.019$) of Fig. 18. Metallicities are somewhat larger for evolutionary models assuming increased abundance of the α -elements (see labels in Fig. 18). Conclusion is the same as for the BaSTI tracks. Only the least massive model A ($M = 0.50 M_{\odot}$) can be matched with the evolutionary tracks.

Luminosities of models B and C are much too high for their masses if confronted with the evolutionary tracks. Consequently, model A is our best model for BLG184.7 133264, selected based on both the pulsation computations and the evolution theory.

5 DISCUSSION AND CONCLUSIONS

In this paper we report the discovery of the first BL Her star showing the regular alternations of the light curve

– the period doubling. The star was discovered nearly twenty years after existence of such objects was predicted by Buchler & Moskalik (1992), who found the period doubling behaviour in their radiative, BL Her-type models. The star, BLG184.7 133264, was found in the Galactic bulge OGLE-III survey data. It pulsates in the fundamental mode, with period equal to 2.4 d. Its Fourier decomposition parameters firmly place it among BL Her variables. We also identified another strong period doubling candidate (BLG189.6 137529) in which however, the amplitude of alternations is very low and more accurate observations are necessary to confirm the detection.

Discovery of period doubling in a BL Her star provides a motivation for in-depth theoretical study of the phenomenon. In particular, the computation of new models, with up to date physics and including the convective energy transfer is of great value. In this paper we present the results

of initial model survey, which is focused on reproducing the period doubling behaviour in BLG184.7 133264. Thus, all computed models have $P_0 \approx 2.4$ d and lie along an approximately straight line in the HR diagram. We have found a large domain, extending over a range of few tenths of solar luminosities, in which period doubling behaviour is possible, with rather large amplitude of alternations, of order of several hundreds of magnitude. The period ratios of the models showing the period doubling effect, indicate the crucial role of the 3:2 resonance between the fundamental mode and the first overtone in causing the period doubling behaviour, confirming the earlier result of Buchler & Moskalik (1992).

The model light curves were transformed into the I -band and compared with the observed light curve of BLG184.7 133264. This was done with the intermediary of the Fourier decomposition parameters. We were able to match the observed pulsation amplitude and the amplitude of the period doubling only for relatively high metallicity, $Z = 0.01$. For three considered model masses, $0.50 M_\odot$, $0.55 M_\odot$ and $0.60 M_\odot$, the model light curves reproduce the observed light curve quite well (Fig. 16). Low order Fourier parameters, R_{21} and ϕ_{21} , are reproduced satisfactorily (particularly for $M = 0.60 M_\odot$). Also the secondary features of the light curve, in particular the pronounced bump at the minimum light are qualitatively reproduced. However, only the lowest mass model ($M = 0.50 M_\odot$) agree with the stellar evolution theory. For $Z = 0.01$ evolutionary tracks for models of $M \geq 0.60 M_\odot$ run well beyond the red edge of the BL Her domain. Consequently, our best estimates for the parameters of BLG184.7 133264 are those of model A (Table 3), specifically $Z = 0.01$, $M = 0.50 M_\odot$ and $L = 168 L_\odot$.

How robust are these estimates? Uncertainties lie in both the pulsation theory and in the evolution theory. Our conclusion about the high metallicity of BLG184.7 133264 is based on the pulsation amplitudes of the computed models. These depend on the adopted convective parameters, in particular on the mixing-length parameter, α , and the eddy viscosity parameter, α_m . As we discussed in Section 3.3.2, change of these parameters is not likely to affect our results strongly. Nevertheless, more extensive model survey, including the variation of other parameters of the turbulent convection model, is needed and planned. In particular, the effect of including the turbulent pressure should be examined.

Derived metallicity can, in principle, be larger than $Z = 0.01$, but only slightly. In test computations with $Z = 0.02$ and assuming convective parameters of set P1, we find no traces of period doubling behaviour (independently of the model mass).

At first glance, metallicity of order of $Z = 0.01$ may seem too high for the Population II object. The metal rich stars, however, are not exceptional in the Galactic bulge. Photometric metallicity estimates for several Type II Cepheids in the bulge range from -1.4 to $+0.6$, with mean value of $[\text{Fe}/\text{H}] = -0.6 \pm 0.17$ (Harris & Wallerstein 1984; Wallerstein 2002). Spectroscopic metallicity determinations, available mostly for bright K and M giants and Red Clump stars, indicate a large spread of metallicities in the bulge, too, with $[\text{Fe}/\text{H}]$ varying from -1.3 to $+0.5$ (see Zoccali 2010, for recent review). $[\text{Fe}/\text{H}]$ determination for several main sequence stars in the bulge was also possible, during the microlensing events (Bensby et al. 2010). For these

stars, metallicity range form -0.7 to $+0.5$. Metallicity can also be estimated for the RR Lyrae stars pulsating simultaneously in the fundamental and the first overtone modes (RRd stars). The OIII-CVS (Soszyński et al. 2011) lists several bulge RRd stars with unusually short periods and low period ratios, down to $P_0 \approx 0.35$ d and $P_1/P_0 \approx 0.726$. The existence of these stars may be explained by high metal abundances, up to $[\text{Fe}/\text{H}] \approx -0.36$. As $Z = 0.01$ corresponds to $[\text{Fe}/\text{H}] \approx -0.27$, we see that our estimate of metallicity of BLG184.7 133264 is not unreasonable.

For the luminosity, we can firmly indicate its lower limit. The period doubling domain in the HR diagram always coincide with the crossing of the 3:2 resonant line with the $P_0 = 2.4$ d line. Run of the two lines shows very little sensitivity to the values of the convective parameters (Section 3.2), as well as to the mass and metallicity of the models (Fig. 10). The lowest luminosity at which the crossing occurs is $\approx 150 L_\odot$.

Based on the recent evolutionary tracks, we have constrained the mass of BLG184.7 133264. With metallicity of $Z = 0.01$ only the models in a narrow mass range of $\approx 0.50 - 0.53 M_\odot$ evolve through the BL Her pulsation domain. We get the best match with the pulsation models for $M = 0.50 M_\odot$. We note however, that at $Z = 0.01$ the evolutionary tracks that cross the BL Her domain vary rapidly with mass of the models. Although the current evolutionary tracks of several groups lead to the same conclusions (Section 4), the systematic errors in the micro-physics (e.g. opacities) or in the treatment of physical phenomena (e.g. convection, rotation, mass loss) may effect the results of evolutionary computations and somewhat change the best matching mass for BLG184.7 133264.

Hydrodynamic model surveys (Buchler & Moskalik 1992, this work) indicate that period doubling phenomenon should be a rather common property of the BL Her stars, at least of those with periods close to 2.4 d. Buchler & Moskalik (1992) found the period doubling behaviour in a period range of 2.0 – 2.6 d. Predicted amplitudes of alternations are usually large, much larger than observed in BLG184.7 133264. Thus, alternations should be easily detectable. Currently, around 250 BL Her variables are known; 55 stars are listed in GCVS (Samus et al. 2009) and close to 200 in OIII-CVS (Soszyński et al. 2008, 2010, 2011, in prep.). OGLE observations are accurate enough to discover alternations with amplitudes as low as a few mmag. Hence, it is somewhat surprising that BLG184.7 133264 is, at the moment, the only BL Her star with firmly detected period doubling behaviour. We note, that our strong period doubling candidate, BLG189.6 137529, also has a period in the expected range. On the other hand, only few of the known BL Her stars have periods close to 2.4 d. Our study shows that higher metallicity (e.g. close to solar, which may not be exceptional for BL Her stars) may inhibit the period doubling effect. Definitely, more detailed non-linear study is needed.

In the forthcoming paper we plan to study the full grid of models, covering the whole BL Her domain in the HR diagram, not only the 2.4 d models. Such survey will reveal the structure of the period doubling domain in the HR diagram, in particular the periods at which the phenomenon is possible and factors which control the existence and strength of the period doubling effect.

ACKNOWLEDGMENTS

Model computations presented in this paper have been conducted on the psk computer cluster in the Copernicus Centre, Warsaw, Poland. RS is supported by the Austrian Science Fund (FWF project AP 21205-N16). The research leading to these results has also received funding from the European Research Council under the European Community's Seventh Framework Programme (FP7/2007-2013)/ERC grant agreement no. 246678.

REFERENCES

- Alard C., Lupton R.H., 1998, *ApJ*, 503, 325
 Alexander D.R., Ferguson J.W., 1994, *ApJ*, 437, 879
 Asplund M., Grevesse N., Sauval A.J., Allende Prieto C., Kiselman, D., 2004, *A&A*, 417, 751
 Baranowski R. et al., 2009, *MNRAS*, 396, 2194
 Bensby T., et al., 2010, *A&A*, 512, A41
 Buchler J.R., Kolláth Z., 2001, *ApJ*, 555, 961
 Buchler J.R., Kovács G., 1987, *ApJ*, 320, L57
 Buchler J.R., Moskalik P., 1992, *ApJ*, 391, 736
 Buchler J.R., Moskalik P., Kovacs G., 1990, *ApJ*, 351, 617
 Buchler J.R., Yecko P.A., Kolláth Z., 1997, *A&A*, 326, 669
 Carson R., Stothers R., 1982, *ApJ*, 259, 740
 Chiosi, C., Bertelli G., Bressan A., 1992, *Ann. Rev. Astr. Astrophys.*, 30, 235
 Dorfi E.A., Feuchtinger M., 1999, *A&A*, 348, 815
 Dotter A., Chaboyer B., Jevremovic D., Kostov V., Baron E., Ferguson J.W., 2008, *ApJS*, 178, 89
 Fadeyev Y.A., Fokin A.B., 1985, *Ap&SS*, 111, 355
 Feuchtinger M., 1999, *A&A*, 351, 103
 Gingold R.A., 1985, *MmSAI*, 56, 169
 Girardi L., Bressan A., Bertelli G., Chiosi, C., 2000, *A&A Suppl. Ser.*, 141, 371
 Grevesse N., Noels A., 1993, in *Origin and Evolution of the Elements*, eds. Pratzio N., Vangioni-Flam E. & Casse M., Cambridge Univ. Press., p. 15
 Harris, H.C., Wallerstein G., 1984, *AJ*, 89, 379
 Hodson S.W., Cox A.N., King D.S., 1982, *ApJ*, 253, 260
 Kolenberg K. et al., 2010, *ApJ*, 713, L198
 Kolláth Z., Molnár L., Szabó R., 2011, *MNRAS*, 412, 1111
 Kovács G., Bucher J.R., 1988, *ApJ*, 334, 971
 Kovács G., Kanbur S., 1998, *MNRAS*, 295, 834
 Kuhfuß R., 1986, *A&A*, 160, 116
 Kurucz R.L., 2005, *Mem. S.A.It. Suppl.*, 8, 14
 Majaess D.J., Turner D.G., Lane D.J., 2009a, *MNRAS*, 398, 263
 Majaess D.J., Turner D.G., Lane D.J., 2009b, *Acta Astron.*, 59, 403
 Marconi M., Di Criscienzo M., 2007, *A&A*, 467, 223
 Moskalik P., Bucher J.R., 1990, *ApJ*, 355, 590
 Moskalik P., Bucher J.R., 1991, *ApJ*, 366, 300
 Moskalik P., Bucher J.R., 1993a, *ApJ*, 406, 190
 Moskalik P., Bucher J.R., 1993b, *Ap&SS*, 210, 301
 Moskalik P., Bucher J.R., Marom A., 1992, *ApJ*, 385, 685
 Pietrinferni A., Cassisi S., Salaris M., Castelli F., 2006, *ApJ*, 642, 797
 Richtmyer R.D., 1957, in *Difference Methods for Initial Value Problems*, Interscience, New York
 Samus N.N. et al., 2009, *yCat....102025S*
 Seaton M., 2005, *MNRAS*, 362, L1
 Smolec R., 2009a, *EAS Publications Series*, 38, 175
 Smolec R., 2009b, PhD Thesis, N. Copernicus Astronomical Centre, Warsaw
 Smolec R., Moskalik P., 2008, *Acta Astron.*, 58, 193
 Smolec R., Moskalik P., Kolenberg K., Bryson S., Cote M.T., Morris R.L., 2011, *MNRAS*, 414, 2950
 Soszyński I. et al., 2008, *Acta Astron.*, 58, 293
 Soszyński I. et al., 2010, *Acta Astron.*, 60, 91
 Soszyński I. et al., 2011, *Acta Astron.*, 61, 1
 Stellingwerf R.F., 1974, *ApJ*, 192, 139
 Stellingwerf R.F., 1974, *ApJ*, 195, 441
 Strom S.E., Strom K.M., Rood R.T., Iben I., 1970, *A&A*, 8, 243
 Szabados L., 2010, in “Variable Stars, the Galactic Halo and Galaxy Formation”, Eds. Sterken C., Samus N., Szabados L., p. 37
 Szabó R. et al., 2010, *MNRAS*, 409, 1244
 Trampedach R., Stein R.F., 2011, *ApJ*, 731, 78
 Udalski A., 2003, *Acta Astron.*, 53, 291
 Udalski A., Szymański M.K., Soszyński I., Poleski R., 2008, *Acta Astron.*, 58, 69
 Wallerstein G., 2002, *PASP*, 114, 689
 Wils P., Otero S.A., 2008, *JAAVSO*, 36, 29
 Woźniak P.R., 2000, *Acta Astron.*, 50, 421
 Wuchterl G., Feuchtinger M.U., 1998, *A&A*, 340, 419
 Yi S., Demarque P., Oemler A., 1997, *ApJ*, 486, 201
 Zoccali M., 2010, *IAUS*, 265, 271